Miner Deposita (2007) 42:551–581
DOI 10.1007/s00126-007-0123-9

ARTICLE

Architecture and emplacement of the Nebo–Babel gabbronorite-hosted magmatic Ni–Cu–PGE sulphide deposit, West Musgrave, Western Australia

Zoran Seat · Stephen W. Beresford · Benjamin A. Grguric · Rob S. Waugh · Jon M. A. Hronsky · M. A. Mary Gee · David I. Groves · Charter I. Mathison

Received: 1 June 2006 / Accepted: 16 January 2007 / Published online: 27 February 2007

Abstract The Nebo–Babel Ni–Cu–platinum-group element (PGE) sulphide deposit in the West Musgrave Block, Western Australia, is the largest nickel sulphide discovery in the last 10 years. The deposit is hosted within a concentrically zoned, olivine-free, tube-like (chonolithic), gabbronorite intrusion associated with the, approximately, 1,078-Ma Giles Complex-layered intrusions in the Warakurna large igneous province. Emplaced into sulphide-free amphibolite facies orthogneiss, the fault-offset Nebo–Babel chonolith extends for 5 km and has a cross-section of 1× 0.5 km. Igneous mineralogy, fabrics, and textures are well preserved. The lithostratigraphy includes variably textured leucogabbronorites (VLGN) that form an outer shell around mineralised gabbronorite (MGN), with barren gabbronorite (BGN) and oxide–apatite gabbronorite (OAGN) in the middle and lower parts of the chonolith. Mineral and whole-rock geochemistry indicate that the units become progressively evolved in the order: VLGN, MGN, BGN, and OAGN, and that incompatible trace-element concentrations increase downwards within the MGN and BGN. The mineralisation, which is confined to the early, more primitive units (VLGN and MGN), occurs as massive sulphide breccias and stringers and as disseminated gabbronorite-hosted sulphides. The massive sulphides were emplaced late in the intrusive sequence, have different PGE chemistry and Cu tenor to the disseminated sulphides, and have undergone sulphide fractionation. The distribution of disseminated sulphides, which are primary magmatic in origin, is related to chonolith geometry and magma flow regimes, rather than to gravitational settling. Sulfur-bearing country rocks are absent in the Nebo–Babel deposit area, and thus, local crustal S addition was unlikely to have been the major mechanism in achieving sulphide immiscibility. The Nebo–Babel intrusion is part of an originally continuous magma chonolith with multiple and related magma pulses. The parental magma was medium- to low-K tholeiite with 8–9 wt% MgO. The initial magma pulse (VLGN), the most primitive and sulphide saturated, was probably emplaced along a linear weakness in the country rock. After crystallisation of VLGN, marginally more fractionated, sulphide-saturated magma was injected through the thermally insulated core of the conduit, forming the MGN. Successive pulse(s) of more fractionated magma (BGN) were emplaced in the core of the intrusion. After magma flow ceased, closed system crystal fractionation produced consistent mineral and chemical fractionation trends within BGN and OAGN. After crystallisation, the intrusion was overturned and then offset by the Jameson Fault resulting in the apparent 'reverse' chemical and mineral trends in Nebo–Babel.

Keywords Nebo–Babel · Musgrave block Australia · Ni–Cu–PGE · Magmatic sulphide deposit

Editorial handling: P. Lightfoot

Z. Seat (✉) · M. A. M. Gee · D. I. Groves · C. I. Mathison
Centre for Exploration Targeting,
School of Earth and Geographical Sciences,
The University of Western Australia,
35 Stirling Highway,
Crawley, WA 6009, Australia
e-mail: seatz01@student.uwa.edu.au

S. W. Beresford · B. A. Grguric · R. S. Waugh · J. M. A. Hronsky
BHP Billiton—Minerals Exploration,
Level 34 Central Park , 152–158 St Georges Terrace,
Perth, WA 6000, Australia

Introduction

The Nebo–Babel Ni–Cu–platinum-group element (PGE) sulphide deposit, discovered in 2000, is the most significant nickel sulphide discovery in the last 10 years. The deposit is hosted within a complex, concentrically zoned, tube-like (chonolithic) gabbronorite intrusion in the, approximately, 1,078-Ma Giles Complex, West Musgrave, Western Australia (Figs. 1 and 2). Nebo–Babel is the first significant discovery of nickel sulphide deposit associated with the Giles Complex in the recently recognised Warakurna large igneous province (LIP) across central Australia (Wingate et al. 2004; Morris and Pirajno 2005), now making the Musgrave Block a prime target for nickel sulphide exploration. The deposit has several distinguishing features including: (1) the chonolithic geometry and presence of massive sulphides along the upper contact, the latter suggesting late-stage dynamic sulphide emplacement typical of large non-komatiitic nickel sulphide deposits, (2) the notable absence of sulphides in country rocks suggesting distal S-saturation, and (3) a low-MgO, tholeiitic host intrusion whose characteristics are similar to those of the Voisey's Bay host intrusion. As a result of these geological features, the mineralised Nebo–Babel system provides an excellent case study to assess the controls on the architecture, emplacement, and genesis of large non-komatiitic nickel sulphide deposits and an opportunity to critically evaluate the controversial controls on S-saturation and nickel sulphide localisation for such deposits.

This work forms part of a multidisciplinary assessment of the deposit (Seat, in preparation). In this paper, new field, petrographical, mineralogical, and geochemical data from the Nebo–Babel deposit and host intrusion are presented, and the intrusive architecture and controls on localisation of nickel sulphides are discussed.

History of discovery

In 1995, the West Musgrave Block in Western Australia was targeted by WMC Resources (purchased by BHP Billiton in 2005) with the objective of discovering a major greenfields Ni–Cu–PGE sulphide deposit similar to that at Voisey's Bay, Canada (e.g. Li and Naldrett 1999). After the selection of target zones, the ground was acquired in 1996, and by mid-1999, reconnaissance exploration led to the recognition of a coincident geochemical, magnetic, and gravity anomaly. Follow-up ground work in 2000 outlined a significant east–

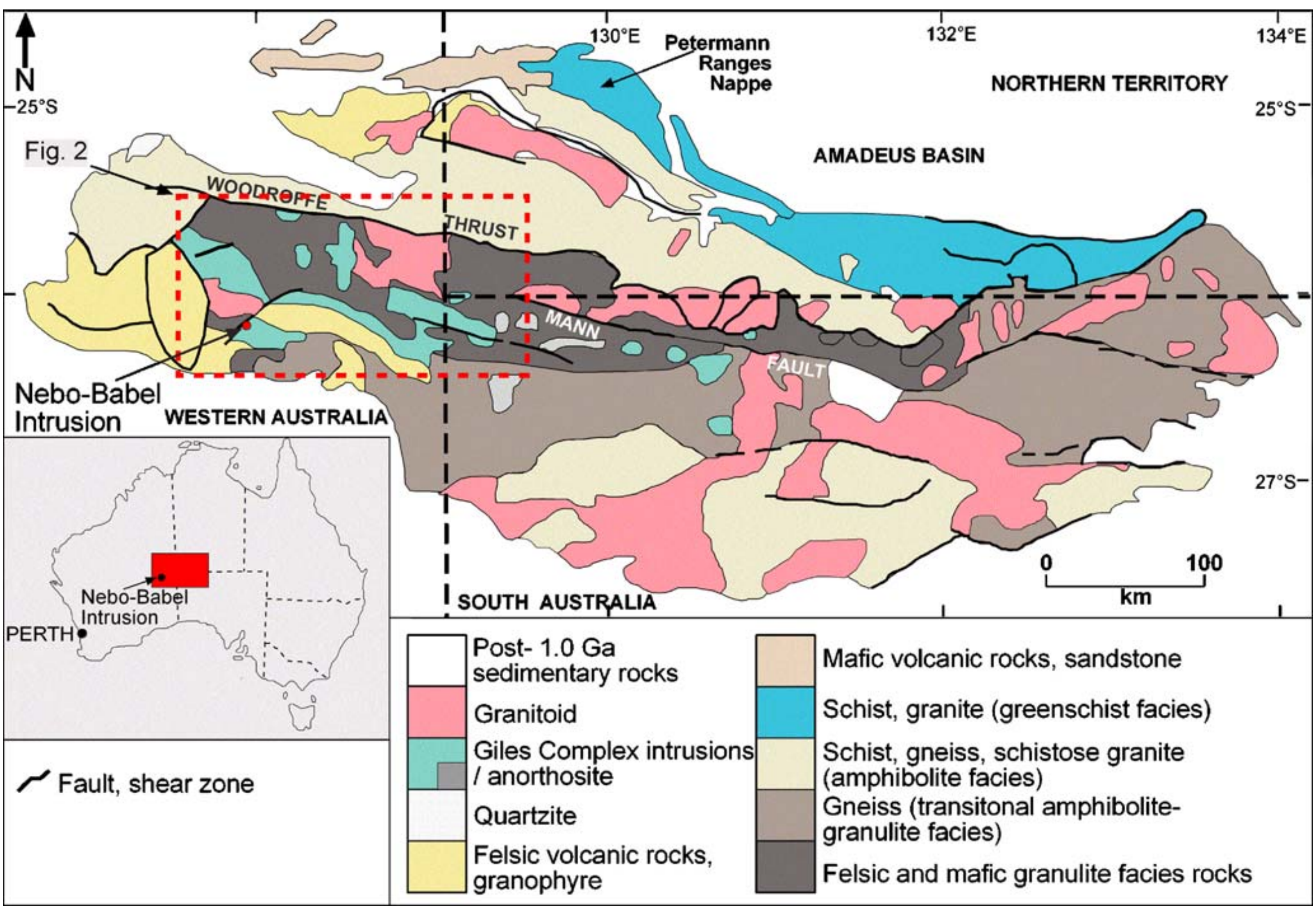

Fig. 1 Regional geology of the Musgrave Block (modified after Glikson et al. 1995). *Dashed outline* shows outline of Fig. 2

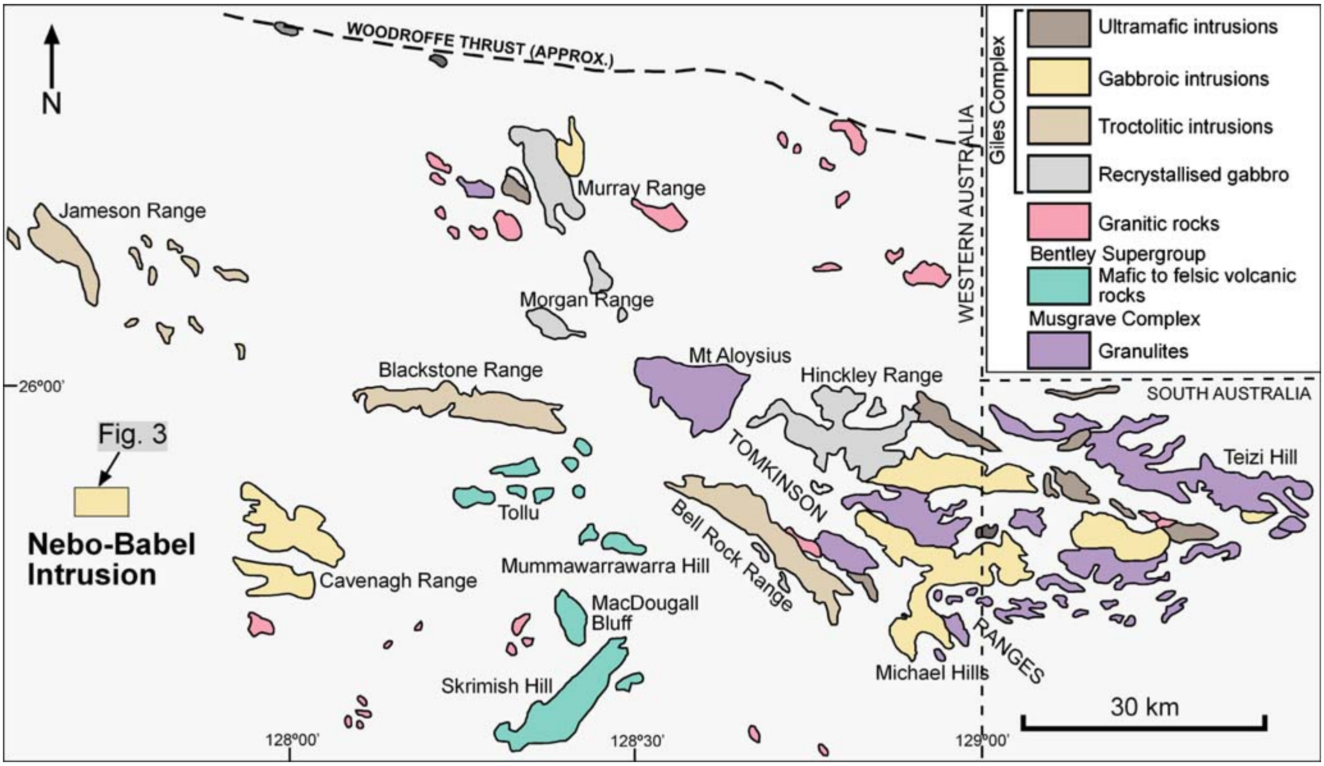

Fig. 2 Simplified geological map of the Tomkinson Ranges–Blackstone–Jameson Area in the West Musgrave Block, showing the regional distribution of the Giles Complex Intrusions and the location of the Nebo–Babel intrusion (modified after Glikson et al. 1995)

west trending electromagnetic conductor that extended intermittently for more than 5 km: the Nebo–Babel nickel sulphide deposit. A more detailed history of the discovery is presented by Baker and Waugh (2005).

Two holes drilled in 2000 intersected 148.9 m of predominantly disseminated mineralisation grading 0.30% Ni and 0.42% Cu at Babel and 26.55 m of massive sulphides grading 2.45% Ni and 1.78% Cu at Nebo. Following these results, a major exploration and resource-definition drilling program, including a 200-m spaced grid of 90-diamond drill holes, was completed in 2001–2002.

More than 11,000 drill core samples were collected and assayed for the purposes of geological and resource model definition. Initial lithostratigraphic subdivisions, descriptions of the intrusive rock units, and an initial geological model based on the drill core mapping and assay results were presented as an internal WMC Resources report by V. R. Goodgame in 2002.

Geological setting

The Musgrave Block is a Mesoproterozoic, east–west trending orogenic belt in central Australia (Fig. 1). It comprises a variety of high grade (amphibolite to granulite facies) basement lithologies overprinted by several major tectonic episodes (e.g. Myers et al. 1996) and intruded by granitoid plutons, layered mafic to ultramafic intrusions of the Giles Complex and mafic dykes (Fig. 2; Nesbitt et al. 1970; Ballhaus and Glikson 1995). A simplified geological history of the Musgrave Block is summarised in Table 1, and specific geological aspects are discussed in more detail below.

Detailed reviews of the Musgrave Block are provided by Glikson et al. (1995) and Glikson et al. (1996, and references therein). Glikson et al. (1996) reviewed the geology of the West Musgrave Block and the Giles Complex, Camacho (2002) and Scrimgeour et al. (2005) studied structural and metamorphic aspects, whereas Sun et al. (1996) and White et al. (1999) presented geochronological data. Petrological and geochemical aspects of the Giles Complex intrusions are provided in Goode (1977), Goode and Moore (1975), Gray and Goode (1989), Ballhaus and Berry (1991), and Ballhaus and Glikson (1995).

Basement

The oldest basement lithologies in the Musgrave Block (which also host the Giles Complex) are amphibolite to granulite facies felsic gneisses with predominantly igneous (intrusive and volcanic) and rare sedimentary protoliths (Daniels 1974). All basement lithologies are characterised by the scarcity of sulfur-bearing minerals, and whole-rock S concentrations are generally <100 ppm (Glikson et al. 1995). Zircons from the basement gneisses give protolith

Table 1 Simplified geological history of the Musgrave Block

Age (Ma)	Magmatic event	Tectonic event	Metamorphic event
1,550–1,300	Felsic (1,502±14 Ma[a]) and minor basic volcanism	Intracratonic extension	Amphibolite to granulite facies metamorphism
~1,200	Kulgera suite granitoids (including charnokites) 1,185±5 Ma[b,c,d]	Intracratonic reactivation	Amphibolite to granulite facies metamorphism (T >750°C; P=5±1 kb)
1,080–1,050	Warakurna LIP[e] ~1,100 Ma Type A dolerite dyke suite[c] Giles Complex Intrusions 1,078±3 Ma[c] Nebo–Babel[f] Tollu Volcanics 1,078±3 Ma[c] Granitic dyke suites 1068±6 Ma; 1,052±11 Ma	Possible major uplift in the western part of the Block	Emplacement P=6±1 kb; lower pressures in the western part of the Block Local recrystallisation of the intrusive lithologies
~1,000	NE-trending Type C olivine–dolerite dyke suite[c]		
~800	NW-trending Type B quartz–dolerite dykes[c]	Rifting of Rodinia	
~550		Petermann Orogeny	Locally high pressure conditions (T~650°C, P=12 kb)

[a] Rb–Sr whole-rock isochron ages by Gray (1978)
[b] U–Pb on zircons by Mabuko et al. (1996)
[c] U–Pb on zircons by Sun et al. (1996)
[d] U–Pb on zircons by White et al. (1999)
[e] U–Pb on zircons by Wingate et al. (2004)
[f] Nebo–Babel placed here based on field, mineralogical, and chemical relationships with the Giles Complex

ages of 1,600–1,540 Ma in the central parts of the Musgrave Block and 1,330–1,300 Ma in the western parts (sensitive, high-resolution, ion microprobe [SHRIMP] U–Pb zircon ages; Camacho and Fanning 1995). Granitoid plutons, which spatially dominate the region, are known as the Alcurra (Kulgera) suite and are associated with the waning stages of the Musgrave Orogeny at 1,190–1,120 Ma (SHRIMP U–Pb zircon ages; Scrimgeour et al. 1999). They also host the Giles Complex. All of the basement lithologies were metamorphosed to amphibolite to granulite facies during the Musgrave Orogeny at 1,200–1,160 Ma (Gray and Compston 1978; Clarke et al. 1995).

The Giles Complex

The Giles Complex consists of a series of partly deformed and recrystallised, layered mafic–ultramafic intrusions, mafic and felsic dykes, and coeval mafic and felsic volcanic rocks (Nesbitt et al. 1970; Daniels 1974; Ballhaus and Glikson 1989; Glikson et al. 1996). The Complex is one of the world's most extensively exposed suites of layered mafic–ultramafic intrusions emplaced at high pressures, 6 to 12 kbar (16 to 33 km; Ballhaus and Berry 1991), in continental crust (Nesbitt et al. 1970; Ballhaus 1993). The depth of emplacement shallows from the north–east westwards across the Musgrave Block, correlating with a change in mineralogy, deep ultramafic-dominated intrusions in the north–east through gabbroids in the central part to shallower troctolite-dominated intrusions (e.g. Jameson–Blackstone Ranges; Fig. 2) in the west. Zircons from the doleritic and gabbroic sills of the Giles Complex, considered to be feeders to some of the layered intrusions (Ballhaus 1993), have SHRIMP U–Pb ages between 1,078±3 Ma and 1,073±5 Ma (Sun et al. 1996). The Tollu Group volcanic rocks are part of the regionally extensive, bimodal, Bentley Supergroup volcanic rocks in the West Musgrave Block (Fig. 2). A rhyolite sample yielded an U–Pb zircon age of 1,078±5 Ma (Sun et al. 1996), which indicates that Tollu Group volcanic rocks are coeval with the Giles Complex intrusions. These intrusions, dyke swarms, and bimodal volcanic rocks are part of the Warakurna LIP across central Australia, interpreted to have been generated by a mantle plume at about 1,075 Ma (Wingate et al. 2004).

Mafic dykes

Multiple generations of mafic dyke swarms (Table 1) intrude and crosscut basement lithologies, granitoids, and the Giles Complex intrusions. Based on field, petrological, and geochemical studies, Clarke et al. (1995) recognised three generations of syn- to post-Giles Complex mafic dykes (types A, B, and C). In addition to these, Nesbitt et al. (1970) recognised four more suites of dolerite dykes in the Tomkinson Ranges (Fig. 2).

Petermann Orogeny

After the emplacement of the mafic dyke suites, a major intercratonic event, the Petermann Orogeny, occurred at about 550 Ma (Scrimgeour et al. 1999; Camacho and McDougall 2000), producing widespread mylonitic fabrics within major shear zones throughout the Musgrave Block (e.g. Camacho et al. 1997). The degree of deformation and metamorphism in layered intrusions decreases from east to west (e.g. Glikson et al. 1996).

Materials and methods

Samples for this study were collected from diamond drill core only. Twenty-one drill holes, 11 from Babel and 10 from Nebo, were logged in detail. Representative drill holes were then sampled to include all rock types to represent the diversity of magmatic, metamorphic, and deformation processes, as well as different mineralisation types. The resulting petrographic and chemical data presented here are used to assemble a chemostratigraphy of the intrusive complex and constrain the relationship between Nebo and Babel.

The compositions of pyroxenes, plagioclase, and olivine were determined by the WDS Cameca SX50 microprobe (WDS, wavelength dispersive spectroscopy; 15 kV accelerating voltage, 30 nA beam current, and 30 s counting time) at the Commonwealth Scientific and Industrial Research Organisation (CSIRO) Laboratory, Perth. Smithsonian diopside, hypersthene, plagioclase, and olivine standard analyses indicate that the analytical precision is better than 5%. Additional analyses of plagioclase and pyroxene were determined on the JEOL JSM 6400 scanning electron microscope (SEM) at the Centre for Microscopy and Microanalysis at the University of Western Australia. A Link EDS X-ray analysis system was used with 15 kV accelerating voltage, 5 nA beam current, and a counting time of 60 s. San Carlos olivine standard analyses indicate that the analytical precision is better than 5%.

The compositions of sulphide minerals were determined using the WDS Cameca SX50 microprobe (20 kV accelerating voltage and 20 nA beam current) at CSIRO, Perth. Two standards were used; pentlandite Astimex #36 and Johnson–Matthey Co metal (99.997%) for Ni, Fe, S, and Co, respectively. To verify Ni concentrations in pentlandite and pyrrhotite, CSIRO-Trace was used on selected samples. CSIRO-Trace is a high-precision WDS analytical technique (Robinson et al. 1998), which utilises an accelerating voltage beam current of 35 kV and 450 nA for pentlandite and pyrrhotite, respectively. Standard analyses indicate that the precision of all analyses is better than 5%.

Whole-rock major and trace elements were analysed by X-ray fluorescence (XRF) on fused glass disks and pressed-powder pellets, respectively, at Macquarie University, Sydney, and Ultratrace Laboratories, Perth. Na_2O was determined by inductively coupled plasma (ICP) optical emission spectrometry, and the remaining elements by XRF, using methods of Norrish and Hutton (1969) and Norrish and Chappell (1977). Sulfur was determined by the

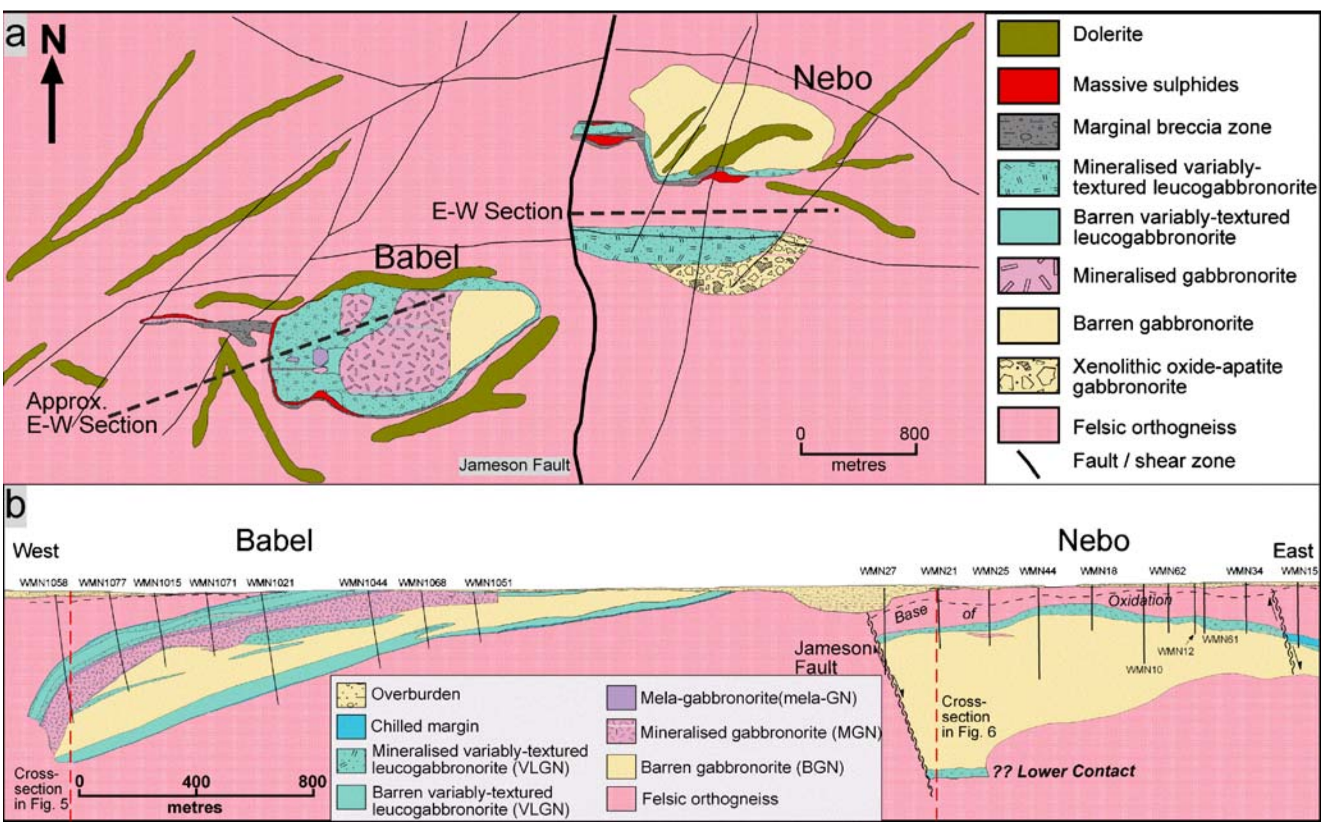

Fig. 3 **a** Surface projection of the gabbronorite rock units, mineralised domains, and major structural elements, **b** longitudinal east–west section though the Nebo–Babel intrusion. Location of cross-sections in Figs. 5 and 6 also shown

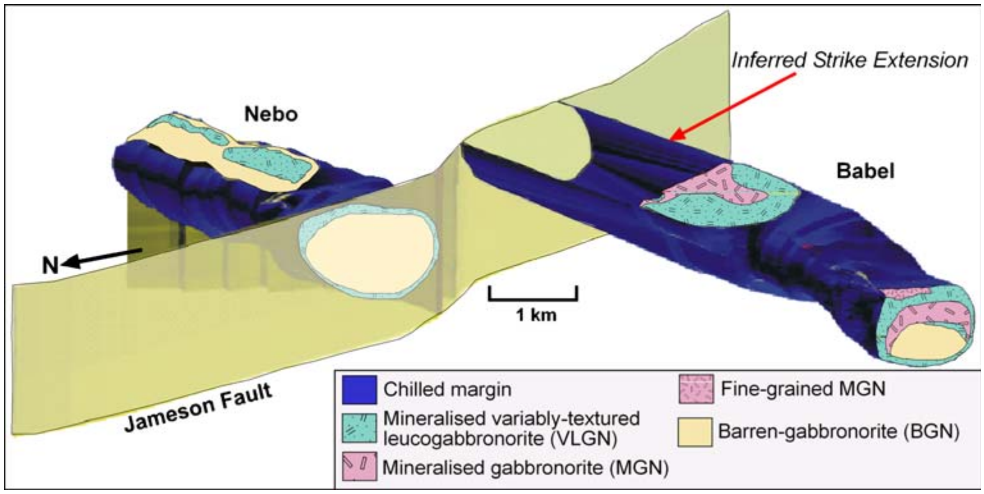

Fig. 4 South–east facing three-dimensional geological model showing spatial and morphological relationships between the Nebo and Babel parts of the intrusion

Leco furnace method. The relative standard deviation is below 2% for all measured oxides.

Thirty Babel–Nebo samples were submitted to Geolabs Geoscience Laboratories, Ontario, for PGE assay (Seat, in preparation). The samples were analysed by fire assay using a Ni sulphide collector followed by an ICP mass spectrometry finish. The method did not include analyses for Os. Analyses of duplicates and published standards indicate that the relative standard deviation is below 5%.

Geology of the Nebo–Babel deposit

The intrusion axis trends in an approximately NNE to E–W direction for 5 km (as currently defined by drilling) has a cross-section of ~1×~0.5 km and is offset by a fault (Figs. 3 and 4). The intrusion has an overall gentle (<10°) WSW plunge and dips to the south at ~15° (Figs. 3 and 4). The deposit is divided into two parts; Babel to the west of the apparently normal fault offset and Nebo to the east. The northern roll-over contact of the intrusion is well constrained along strike, and the tube-like morphology (Fig. 4), both at Nebo and Babel, is demonstrated in the geological cross-sections (Figs. 5 and 6). Drilling does not intersect the down-dip contact to the south. Three-dimensional modelling of the geological and geophysical data (unpublished BHP Billiton data) provides additional constraints on the morphology of the intrusion (Fig. 4). Geological cross-sections (Figs. 5 and 6) and the three-dimensional geological model (Fig. 4) show that Nebo and Babel have almost identical morphology and marginal intrusive rock units. However, the deposits differ in mineralisation styles, rock

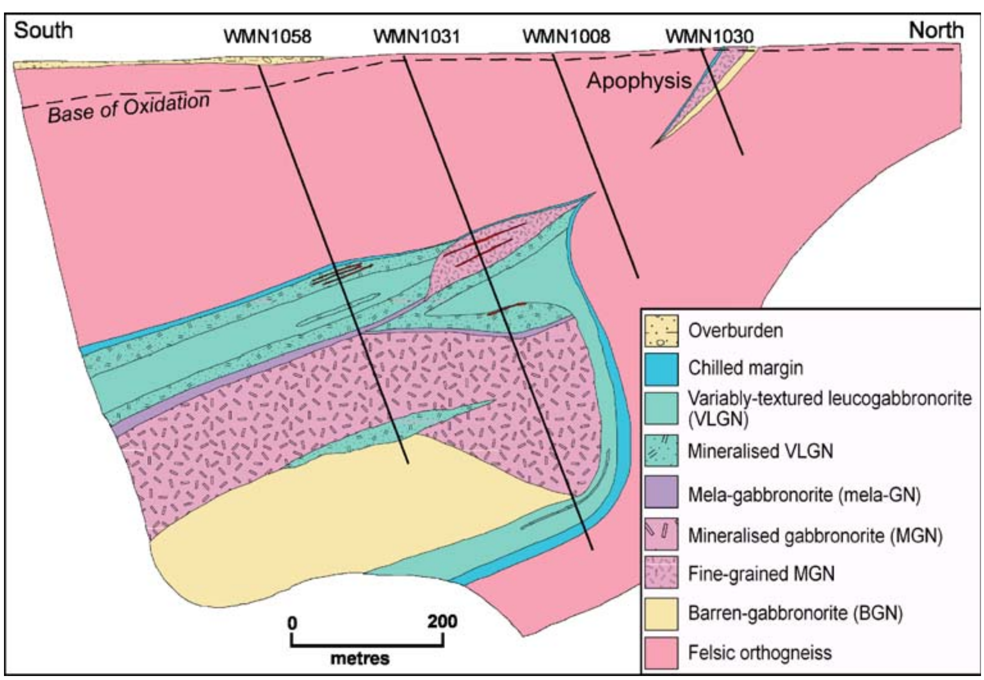

Fig. 5 West-facing geological cross-section through Babel illustrating the northern rollover contact, chonolith morphology, and an apophysis

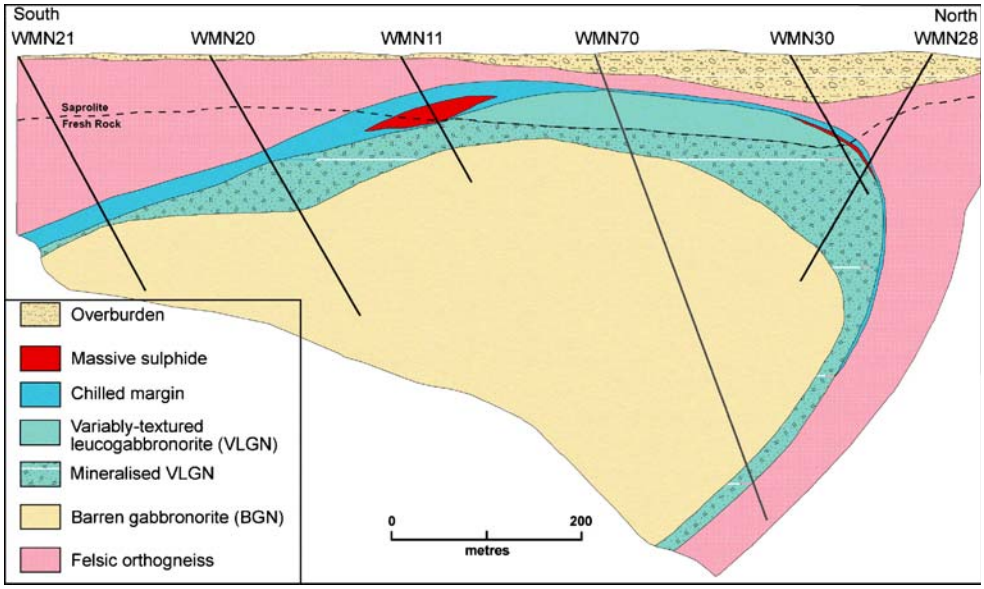

Fig. 6 West-facing geological cross-section through Nebo showing very similar chonolith morphology to Babel

types in the core of the intrusion, and degree of alteration. Consequently, the deposit description below is divided into two parts.

Babel

The Babel part of the intrusion, which crops out at the surface, is first intersected by drilling ~1.7 km west of the fault offset (Fig. 3). The continuation of the eastern part of Babel towards the Jameson Fault is inferred based on geophysical data, as there are no drill holes (Fig. 3b). The intrusion extends further to the west for ~2 km from the first drill hole intersection, and its western end is open down-plunge to the SW (Fig. 3b). The central part at Babel has a plunge of ~ 10°SW, an ~E–W strike orientation, and dips at ~15°S, but the plunge increases to ~25–30°SW, and the strike changes to SW at its western end (Fig. 7). At the northern contact towards the west, there is an apophysis composed of fine-grained, mineralised, layered, gabbronorite (~40×100 m in cross-section), which strikes at ~110° and dips at 30° to 45°S, connects to, and forms a part of the intrusion (c.f. Figs. 5 and 7). Towards west, the apophysis thins, intrudes the country rock, and becomes progressively smaller, ultimately pinching out (Fig. 7).

The sequence of the gabbronorites in the Nebo–Babel intrusion is illustrated in Fig. 8. The dominant rock types

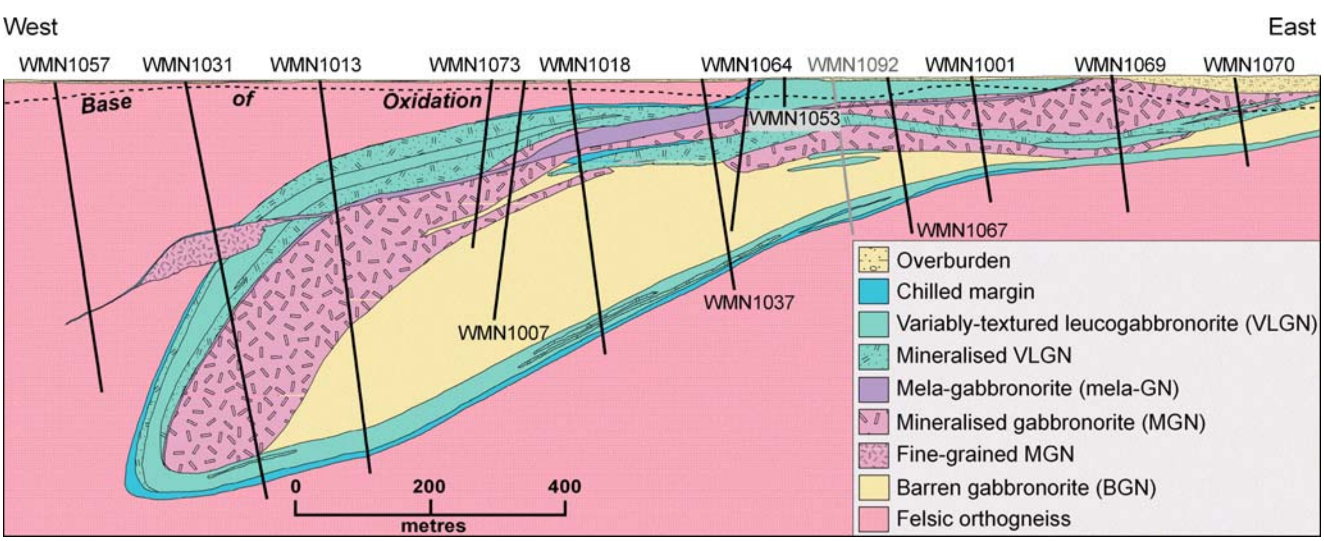

Fig. 7 North-facing, east–west longitudinal section through Babel, which illustrates south westerly plunge, the main units, and decrease in the thickness of the mineralised unit towards the east. Cross-cutting dykes omitted for simplicity. Note that the strike orientation of the intrusion changes to SW at the western end: hence, the western closure in the longitudinal section. See location of WMN 1018 drill hole. Section azimuth 247°, Dip 73°NW

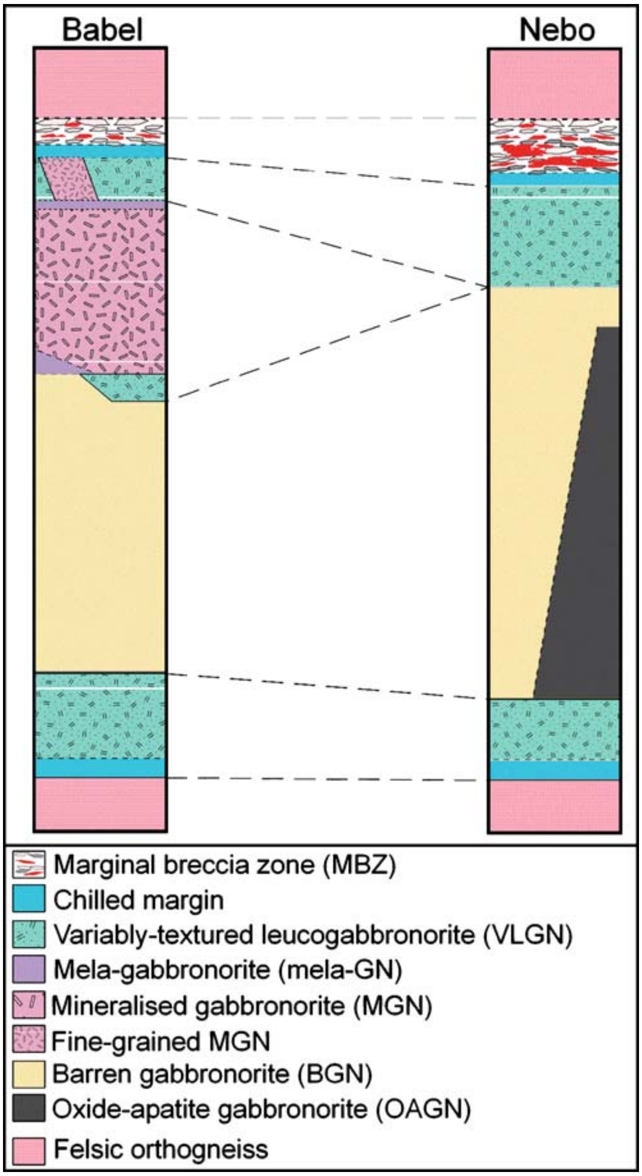

Fig. 8 Schematic illustration of the lithostratigraphy in the Nebo and Babel parts of the intrusion

are the barren and mineralised gabbronorites (MGN) followed by barren and mineralised leucogabbronorites.

The felsic orthogneiss country rock comprises predominantly equal proportions of K-feldspar, plagioclase, and quartz, with minor amphibole, biotite, ilmenite, apatite, and trace orthopyroxene (Fig. 9a,b). Sulphides are not recorded from the country rock in the Nebo–Babel area. The marginal breccia zone (MBZ) is best developed at the upper contact between the country rock felsic orthogneiss and the chilled margin of the intrusion. The MBZ is <3 m thick, continuous along strike of the intrusion, and comprised of sub-rounded felsic orthogneiss inclusions, massive sulphide clasts, and, locally, medium-grained gabbronorite enclaves that are hosted in a predominantly sulphide, and, less commonly, fine-grained gabbronorite or orthogneiss matrix (Fig. 9b). The orthogneiss inclusions are generally partly resorbed, which suggests that they have reacted with the enclosing sulphide or gabbronorite matrix. Orthogneiss rafts, which vary in thickness from 10 to 120 cm, also occur within the MBZ. The rafts contain pyrrhotite and chalcopyrite that appear on textural grounds to have infiltrated and replaced the original orthopyroxene, amphibole, or biotite crystals.

The contacts between the MBZ and the chilled margin rock unit are generally gradational and best defined by finer grain size and the near-absence of gneissic and massive sulphide inclusions in the latter. The chilled margin comprises fine-grained gabbronorite, which locally contains sulphide globules and partly, to fully, resorbed gneiss xenoliths (Fig. 9c). There is no thermal aureole within the orthogneiss at the contacts with the upper and basal chilled margins. However, chilled margin apophyses up to 1 m thick extend for several tens of metres into the country rock. Locally, xenoliths of chilled margin rocks occur within the variably textured leucogabbronorite (VLGN). The chilled margin rocks are identical along the upper and basal contacts and become progressively coarser-grained inwards and over 3- to 5-m grade into VLGN. All VLGN units are texturally and mineralogically identical.

The VLGN along the top of the intrusion occurs between the chilled margin and the coarse-grained mela-gabbronorite (mela-GN). The VLGN unit is predominantly barren or, where mineralised, contains disseminated and blebby sulphides (Fig. 9d) that are concentrated within its uppermost part and along the lower contact with the mela-GN (Figs. 5 and 7). Massive sulphide lenses, up to 2 m thick, occur within the VLGN. Only the discovery hole (WMND 7) at Babel intersected a thin (<10 m thick) troctolite layer in the central part of the VLGN at the top of the intrusion. Contact relationships suggest that this troctolite unit is intrusive into the VLGN unit. The VLGN is underlain by mela-GN, which is generally <10 m thick, but locally can reach thicknesses of up to 30 m in the central parts at Babel (Fig. 7). The mela-GN also occurs between the MGN above and barren gabbronorite (BGN) below, and it crosscuts VLGN (Fig. 7). The unit is generally barren, although it locally contains <10 vol.% of disseminated and interstitial sulphides. The mela-GN is interpreted as the lateral equivalent of the fine-grained mineralised gabbronorite (F.G. MGN), which occurs at the northwestern roll-over contact at Babel, between the country rock gneiss and VLGN, and forms an extension to the intrusion (Figs. 5 and 7).

The MGN (Fig. 9e), which contains the bulk of the mineralisation, occurs everywhere at Babel between the mela-GN and BGN (Figs. 5 and 7). The unit is significantly

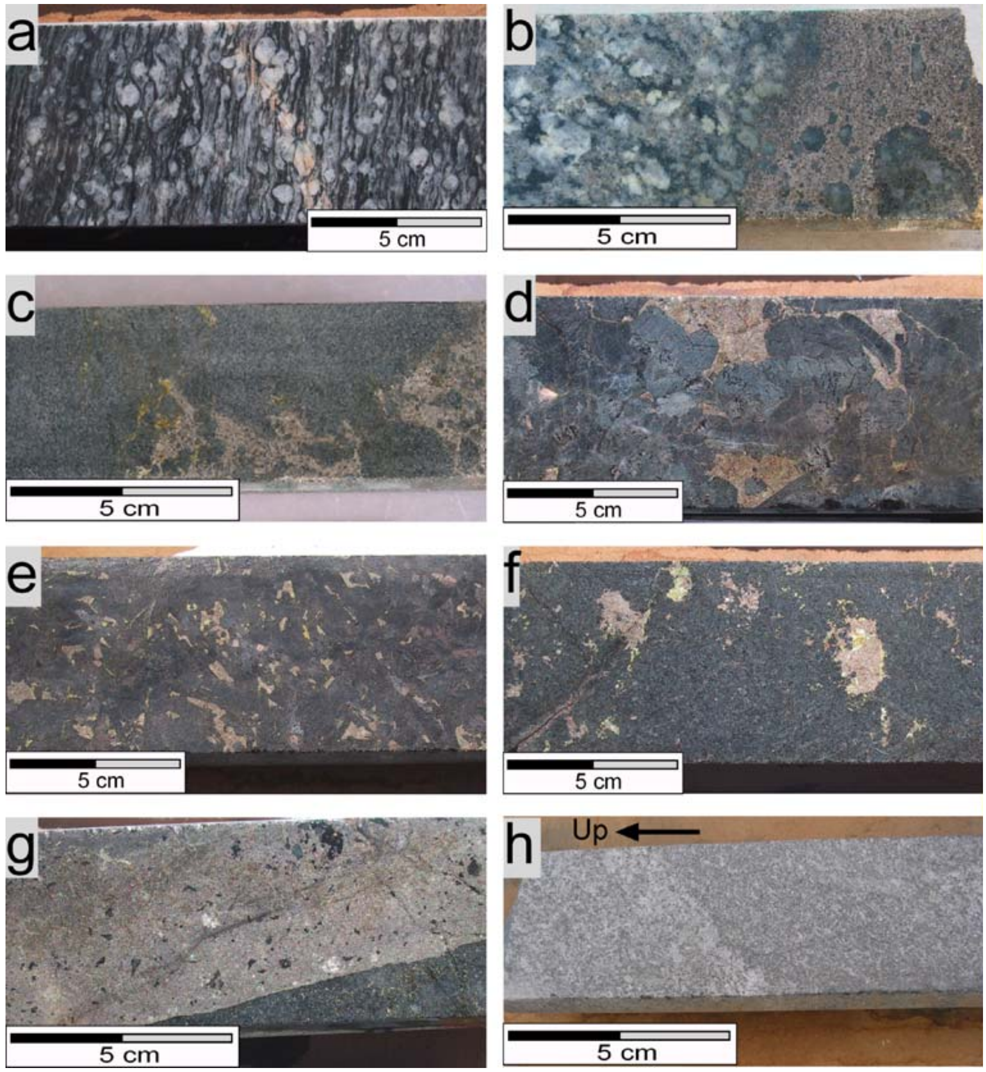

Fig. 9 Photographs of major rock types and textural and mineralogical relationships in the Nebo–Babel intrusion: **a** mylonitic fabric in the orthogneiss WMN1031 drill hole 253.5 m, **b** massive sulphide vein emplaced into, and containing xenoliths of, the orthogneiss, WMN1013 122.1 m, **c** igneous textured sulphides that appear to have intruded chilled margin gabbronorite, WMN1018 44.9 m, **d** magmatic, very coarse disseminated sulphides in coarse grained VLGN, WMN1031 395.3 m, **e** typical disseminated sulphide textures in the MGN, WMN1031 540.0 m, **f** coarse-grained sulphide blebs in F.G. MGN, WMN1031 258.3 m, **g** massive sulphides within F.G. MGN (note gabbronorite xenoliths within the sulphides and a very sharp contact), WMN1031, 271.7 m, **h** an oxide-rich layer within the OAGN (note a relatively sharp upper contact and gradational decrease in oxide abundance downwards), WMN31 363.1 m

thicker at the western end and progressively thins towards the east (Fig. 7). The F.G. MGN is almost identical to the MGN, except for its finer grain size, higher sulphide abundance (up to 30 vol.%), sulphide blebs (Fig. 9f), and locally massive sulphide lenses (Fig. 9g) up to 1 m in width. Based on the gradational contacts between the mela-GN and the underlying MGN, the mela-GN is interpreted as the marginal layer of the MGN.

VLGN also occurs in the central and easternmost parts of Babel between the MGN and BGN and/or within the MGN (Figs. 5 and 7). BGN is volumetrically the dominant rock type at Babel and is very similar to the mineralised variety, but is marked by the absence of sulphides, slightly higher pyroxene abundance, and an igneous foliation defined by plagioclase. Both BGN and MGN are interpreted to contain VLGN rafts (see cross-section in Fig. 5). VLGN, with only minor disseminated sulphides, occurs at the base of the BGN (Fig. 7). The basal contact comprises the same chilled margin rocks as the upper contact, but it lacks the thick MBZ and the sulphide lenses.

Nebo

The Nebo part of the intrusion, which occurs east of the dividing Jameson Fault offset (Fig. 3), extends for ~1.8 km as defined by current drilling. The most easterly drill holes and geophysical data indicate that the intrusion extends further east, but its eastern limit has yet to be defined. Geological cross-sections through Nebo (Fig. 6) confirm its morphological similarity with Babel. The mineralisation consists primarily of massive sulphide lenses that occur along the upper intrusive contact within the MBZ. Compared to Babel, the sequences of disseminated and interstitial sulphides are relatively thin and, at Nebo, occur within the VLGN unit along the top of the intrusion. The igneous sequence developed within Nebo is presented in Fig. 8. Nebo is mineralogically and texturally almost identical to Babel, except for the occurrence of oxide–apatite gabbronorite (OAGN) at its eastern end, the significantly higher proportion of massive sulphide lenses, and the absence of the MGN.

The MBZ at Nebo is a continuous, up to 35 m thick, layer along the upper contact between the orthogneiss and chilled margin (Figs. 6 and 10). Locally, massive sulphide breccia veins occur within the country rock. The majority of sulphide mineralisation within Nebo occurs as MBZ-hosted massive sulphide lenses up to 26 m thick. Except for the significantly higher abundance of massive sulphide lenses, the composition of the MBZ is very similar to Babel. The MBZ grades downwards into chilled margin rocks.

The chilled margin rocks are the same as those at Babel and locally contain sulphide globules. Underlying the upper chilled margin is the VLGN unit, which is interpreted as the lateral equivalent of the VLGN at Babel. The unit is continuous along strike at Nebo (Fig. 10), but is best developed at the western end, near the fault offset, thinning to the east. The VLGN, in WMN 70 drill hole, is intruded by a 16-m wide mineralised troctolite unit. The absence of such units in other drill holes at Nebo suggests that the troctolite layers are not laterally continuous.

VLGN in the middle parts of the intrusion is not recognised at Nebo, and the VLGN is underlain by the BGN, which can locally host trace-disseminated and interstitial sulphide grains along its uppermost part. Those parts of the BGN, which locally contain trace sulphides, are potentially the lateral equivalents of the MGN at Babel. The BGN constitutes most of the section at Nebo, being most dominant within the western and central parts, where it is underlain by the VLGN, but the lower contact has only been intersected at the western end (Fig. 6). The VLGN at the basal contact at Nebo is interpreted to be the lateral equivalent to the VLGN at the base of Babel, although shearing and post-magmatic alteration have significantly modified the lower contact and the adjacent country rocks. BGN thins out towards the east where it is underlain by OAGN (Fig. 8). The OAGN, which is similar to BGN, except that it contains distinct oxide-rich layers (Fig. 9h) with apatite grains, is the most fractionated unit in the intrusion. Drilling has not intersected the lower contact at the eastern end of Nebo. The xenolithic oxide–apatite gabbronorite (XOAGN) is intersected in only one drill hole (Fig. 3a) where it is underlain by OAGN. The unit is similar to the OAGN, except that it contains country rock xenoliths.

Lithostratigraphic relationships

Geological cross-sections and longitudinal sections through the Nebo–Babel intrusion (Figs. 5, 6, 7 and 8, 10) show a detailed lithostratigraphy for the intrusion. The thickness of all units varies along strike and down dip of the intrusion (c.f. Figs. 3b and 7). The VLGN units occur at the margins of the intrusion and are continuous along strike, and across, the Jameson Fault (c.f. Figs. 7 and 10). The thickness of the VLGN along the basal contact is almost constant along strike, whereas at the top of the intrusion it changes across strike at Babel (Figs. 7 and 10), being thickest at the northern roll-over contact at both Babel and Nebo (Figs. 5 and 6). The thickness of the MGN is highly variable, but as a generalisation, the unit is thickest at the western end of Babel and progressively thins out eastwards (Figs. 3b and 7) and is not intersected across the fault at Nebo (Fig. 10). The BGN is intersected everywhere at Babel and Nebo and appears to progressively increase in thickness towards the east, as the thickness of the MGN decreases (Fig. 3b).

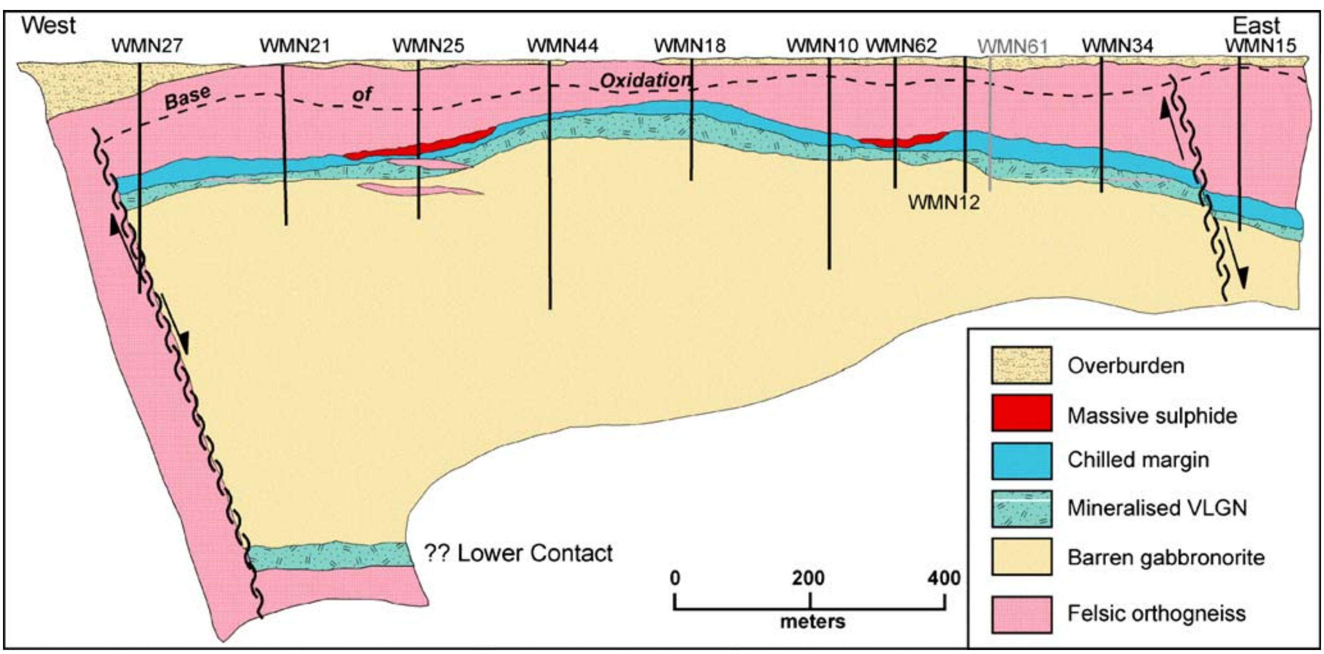

Fig. 10 North-facing, east–west longitudinal section through Nebo that illustrates the main units and the massive sulphide lenses along its upper contact

Table 2 Summary of units within the Nebo–Babel Intrusion

Deposit	Intrusive Phase	Lithostratigraphic unit	Major Minerals (vol.%)	Sulphide (vol.%)	Textures and Fabrics
Babel	Phase I	Chilled margin	Pl 45–55; Opx 20–25; Aug 20–25	<1	f.g., Massive, ophitic
		Marginal microgabbro	Pl 45–55; Opx 20–25; Aug 20–25	<1 to <10	f.g. to m.g., Massive
		VLGN	Pl 65–85; Opx 15–25; Aug 5–10	<1 to 5–20	f.g. to Pegmatoidal, massive
	Phase ?III	MBZ	Pl 10–20; Mc 10–20; Qtz 10–20	60–85	c.g. Massive, deformed
	Phase II	Troctolite	Pl 50–55; Ol 35–40; Opx ~5	<2	c.g., Massive
		MGN	Pl 55–65; Opx 15–25; Aug 5–10	5–25	c.g., Moderate flow foliation
		F.G. MGN	Pl 55–60; Opx 15–25; Aug 5–10	5–30	f.g. Layered
		Mela-gabbronorite	Pl 20–35; Opx 30–45; Aug 20–30	<1 to 5–15	c.g. Massive
	Phase II	BGN	Pl 40–45; Opx 25–35; Aug 20–30	<1	c.g. Strong flow foliation
Nebo	Phase I	Chilled margin	Pl 45–55; Opx 20–25; Aug 20–25	<1	f.g. Pl phyric, ophitic
		Marginal microgabbro	Pl 45–55; Opx 20–25; Aug 20–25	<1 to <10	f.g. To m.g., massive
		VLGN	Pl 65–85; Opx 15–25; Aug 5–10	<1 to 5–20	f.g. To pegmatoidal, massive
	Phase ?III	MBZ	Pl 10–20; Mc 10–20; Qtz 10–20	60–85	c.g. Massive, deformed
	Phase II	Troctolite	Pl 60–65; Ol 30–35; Opx ~5	<2	c.g., Massive
	Phase III	BGN	Pl 40–45; Opx 25–35; Aug 20–30	<1	c.g. Strong flow foliation
		OAGN	Pl 35–45; Opx 15–25; Aug 5–10; Il & Mag 5–10; Ap 4–8	<1	c.g. Very strong flow foliation
		XOAGN	Pl 35–45; Opx 15–25; Aug 5–10; Il & Mag 5–10; Ap 4–8	<1	v.c.g. Deformed, foliated

Mineral symbols in accordance with classification of Kretz (1983)

BGN Barren gabbronorite, *F.G. MGN* fine-grained mineralised gabbronorite, *MBZ* marginal breccia zone, *MGN* mineralised gabbronorite, *OAGN* oxide–apatite gabbronorite, *VLGN* variably textured leucogabbronorite, *XOAGN* xenolithic oxide–apatite gabbronorite

f.g. <1 mm, *c.g.* 5–30 mm, *v.c.g.* >30 mm, *Ap* apatite, *Aug* augite, *Il* ilmenite, *Mag* magnetite, *Mc* microcline, *Ol* olivine, *Opx* orthopyroxene, *Pl* plagioclase, *Qtz* quartz

OAGN is only present at Nebo where it underlies the BGN (Fig. 8), and hence, little is known about the variation in its thickness.

Petrography

All rock types in the Nebo–Babel system are gabbronorites (LeMaitre 2002). Sulphides comprise up to 30 vol.% in the mineralised units, as described below. The most significant mineralogical and textural characteristics of the intrusive rock types are summarised in Table 2 for comparative purposes and are briefly described below. Unless otherwise stated, lithostratigraphic units are mineralogically and texturally identical at Nebo and Babel, and ortho- and clino-pyroxene are referred to as pyroxenes.

The magmatic mineralogy is well preserved at Babel. The following features are recorded in all intrusive units. Plagioclase exhibits incipient to weak saussuritisation along grain boundaries and intra-crystal micro-fractures. Orthopyroxene is strongly pleochroic, and pyroxenes contain opaque to purple-brown inclusions, parallel to the cleavage planes and exsolution lamellae parallel to (001). Locally, pyroxenes show incipient to moderate uralitisation and are rimed by syn- to late-magmatic green and brown hornblende and biotite.

Post-magmatic hydrothermal alteration is locally pervasive at Nebo, and the alteration assemblages are hornblende and cummingtonite, and locally, epidote and scapolite replace plagioclase. The higher degree of alteration is thought to be related to spatially restricted, post-intrusion monzogranite dyke swarms. Additional fluids may have been sourced from the adjacent Jameson Fault zone.

At the hand-specimen scale, primary igneous textures are generally well preserved. However, moderate to extensive syn- to post-magmatic structural overprinting is visible in thin sections and is exemplified by bent plagioclase twin planes, marked fracturing and sub-grain fragmentation and recrystallisation along grain margins. In the most deformed parts, these are very fine-grained (<0.5 mm), recrystallised plagioclase crystals. Fractures and internal microfissures in plagioclase are filled by sulphides in mineralised units. Deformation has produced kink bands in pyroxenes.

Felsic orthogneiss and MBZ

The felsic orthogneiss comprises equal proportions of microcline, plagioclase (calcic oligoclase to andesine), and quartz, comprising 80 to 85 vol.% of the rock, with 15 to 20 vol.% amphibole, biotite, ilmenite, apatite, and trace orthopyroxene. Plagioclase and K-feldspar form up to 20-mm-long megacrysts within recrystallised quartz–feldspar matrix. Sulphide-bearing minerals are absent in the felsic orthogneiss.

Randomly oriented orthogneiss xenoliths, up to 20 mm in length (10 to 35 vol.%), occur in a massive sulphide matrix (60 to 85 vol.%). The sulphides (up to 5 mm) are mainly pyrrhotite, followed by chalcopyrite (up to 40 vol.%) and pentlandite (<10 vol.%). Locally, there are chalcopyrite-rich domains and scattered grains of ilmenite ≫ magnetite up to 2 mm in diameter (≤5 vol.%). The orthogneiss xenoliths, composed of commonly rounded to sub-rounded plagioclase grains (Fig. 11a), are surrounded by smaller aggregates of microcline–quartz granophyric intergrowths. Individual microcline grains are rare. Hornblende and biotite are interstitial, and locally, hornblende forms symplectite-like intergrowths with quartz and microcline, and trace apatite is present. Minor orthogneiss and chilled gabbronorite-hosted breccias, generally, consist of sulphides that have invaded the silicate matrix.

Chilled margins and marginal microgabbros

The chilled margins are massive and locally ophitic gabbronorites (Fig. 11b) that comprise plagioclase (45 to 55 vol.%) and pyroxenes (each 20 to 25 vol.%). Biotite (1 to <3 vol.%) forms rims on pyroxenes and oxides, and trace green-brown hornblende forms blebs within pyroxenes. Ilmenite and magnetite comprise ≤1 vol.%. Generally, there are only trace sulphides, but these can be up to 20 mm in diameter. Country rock xenoliths, up to 50 mm in diameter, commonly with associated sulphides, occur locally.

Chilled margins grade into marginal microgabbros, which are coarser grained (0.1 to 1 mm), and sulphides can locally comprise up to 10 vol.%. Country rock xenoliths with associated sulphides are very rare. Xenoliths of the marginal microgabbros, which occur within the VLGN or MGN, are sulphide-free.

VLGN and troctolites

The VLGN varies from coarse grained (5 to 30 mm) to pegmatitic (> 30 mm), with plagioclase megacrysts in pegmatitic domains up to 100 mm in length. The VLGN consist of randomly oriented plagioclase (65 to 80 vol.%), indicating that this was the predominant liquidus phase, orthopyroxene (15 to 25 vol.%), and clinopyroxene (<5 vol.% to locally >10 vol.%). Rare olivine comprises up to 5 vol.%. In both VLGN and troctolite units, olivine-plagioclase contacts have coronas characterised by an outer discontinuous layer of orthopyroxene intergrowths (Fig. 11c). There are sub-microscopic, light green vermicules of pleonaste, locally within the symplectites. Pale green and pale brown biotite and amphibole are sited between the orthopyroxene layer and pyroxene–plagioclase symplectites. Trace biotite and amphibole rim sulphides, oxides, and pyroxenes. Pale green and pale brown biotite also forms in coronas around olivine. Brown hornblende and pale green actinolite are adjacent to pyroxene grains, and there is minor (<2 vol.%) ilmenite and magnetite. Where mineralised, the VLGN consists of 5–20 vol.% sulphides.

Troctolite at Babel is massive, coarse to very coarse grained (5–30 mm) with partly dendritic olivine (35 to 40 vol.%), plagioclase (50 to 55 vol.%), and intercumulus pyroxenes. Plagioclase–olivine contacts are characterised by coronas as described above. Sulphides and oxides (ilmenite and magnetite) total ~1 vol.%.

Mineralised gabbronorites

There is an abrupt change in grain size and texture from VLGN to MGN, with the latter having a more uniform grain size (5–20 mm) and containing plagioclase that commonly defines a moderate to strong preferred alignment. This unit comprises plagioclase (55 to 65 vol.%), orthopyroxene (15 to 25 vol.%), and clinopyroxene (5 to 10 vol.%). Trace minerals include ilmenite, magnetite, biotite, and apatite that are adjacent to oxides and sulphides (5 to 25 vol.%), which occur as bleb-like aggregates or more commonly are interstitial (Fig. 11d).

Mineralogically, F.G. MGN is identical to the MGN, except for its finer grain size (1–5 mm) and higher proportion of sulphides (up to 30 vol.%). Locally, F.G. MGN has alternating plagioclase-bearing pyroxenite and gabbronorite layers that define small-scale, <300 mm thick, rhythmic layering.

Variably mineralised, mela-GN comprises orthopyroxene (30 to 45 vol.%), clinopyroxene (20 to 30 vol.%), and plagioclase (20 to 35 vol.%). Biotite (<2 vol.%) forms fringes on orthopyroxene, sulphides, and oxides.

BGN and OAGN

BGN is texturally homogeneous with moderate to strong plagioclase alignment. The unit is similar to MGN except that it lacks sulphides (Fig. 11e), and pyroxenes are in approximately equal proportions (25 to 35 vol.%). Biotite

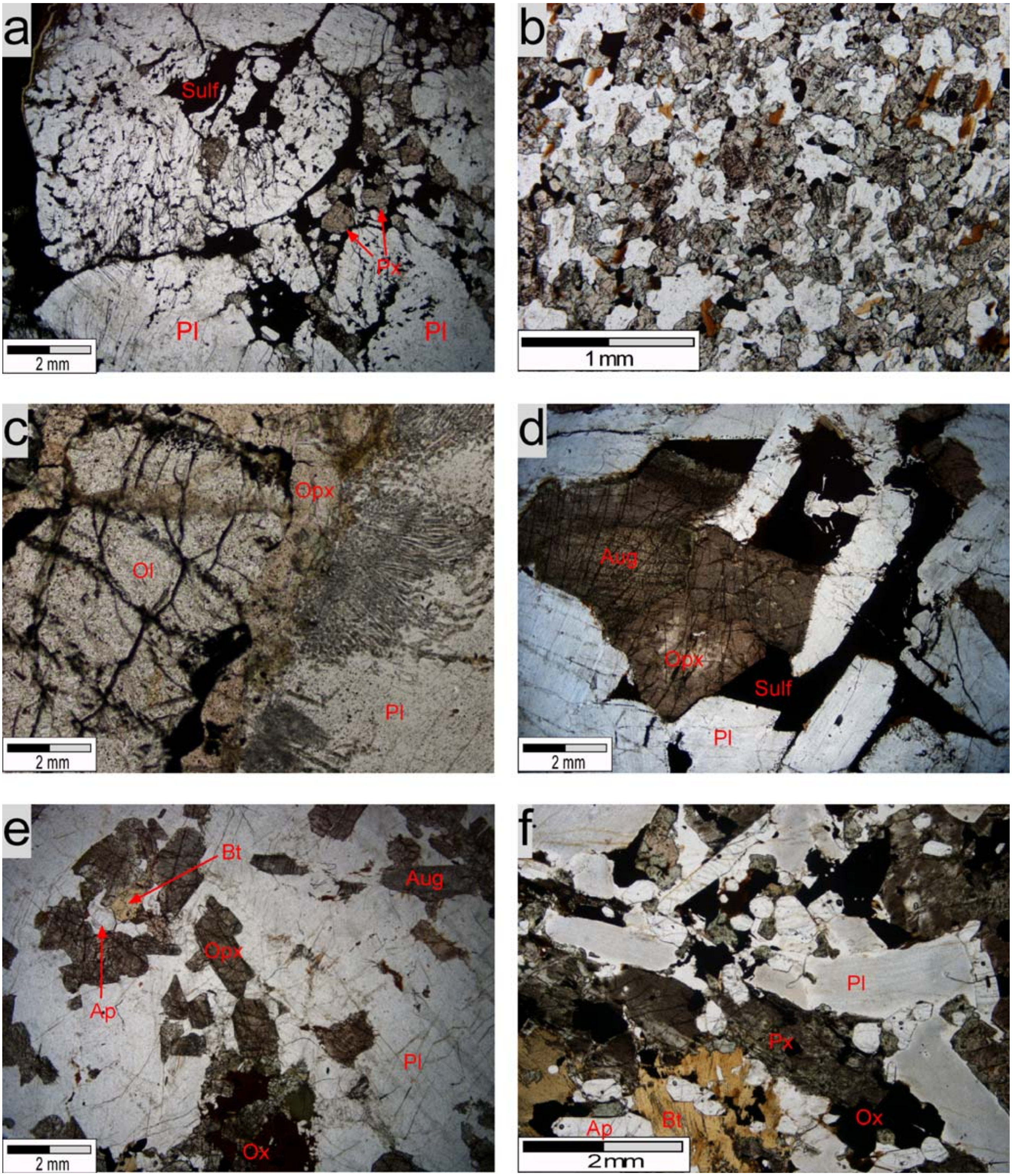

Fig. 11 Photomicrographs (*plane light*) of major rock types in the Nebo–Babel intrusion showing their mineralogical and textural relationships: **a** massive sulphide breccia with orthogneiss plagioclase clasts showing partial resorbtion by the massive sulphide matrix, sample WMN1018 53.5 m, **b** randomly oriented plagioclase, ortho- and clino-pyroxene, ilmenite, magnetite, and biotite in a chilled margin, WMN1031 676.1 m, **c** olivine rimmed by inner corona of orthopyroxene, and by outer radial symplectite intergrowth between orthopyroxene and plagioclase, WMN1092 38.1 m, **d** mineralised gabbronorite with interstitial sulphides, sample WMN1092 88.8 m, **e** oxides, biotite, and apatite in barren gabbronorite, WMN1018 383.5 m, **f** typical oxide–apatite gabbronorite with apatite prisms, oxides, and biotite interstitial to plagioclase and pyroxene, WMN31 300.2 m. *Ap* Apatite, *Aug* augite, *Bt* biotite, *Opx* orthopyroxene, *Ox* oxides, *Pl* plagioclase, *Sulf* sulphide

(< 5 vol.%) and hornblende (1 to 5 vol.%) are more abundant in this unit compared to VLGN and MGN. Apatite (1 to 3 vol.%) and oxides (≤2 vol.%; ilmenite ≫ magnetite) are generally associated with biotite. Granular, late magmatic quartz (<0.5 vol.%, <2 mm) and trace sulphides are also present. BGN at Nebo varies from unaltered to, locally, very uralitised and saussuritised.

The OAGN (Fig. 11f) is medium to coarse grained (10 to 30 mm) with moderate to very strong igneous foliation defined by plagioclase (35 to 45 vol.%). Orthopyroxene (15 to 25 vol.%) is the dominant mafic phase, whereas clinopyroxene (5 to 10 vol.%), generally, encloses inverted pigeonite and contains blebs of brown hornblende. Green and brown hornblendes (1 to 5 vol.%) form rims on pyroxenes. Oxides (ilmenite ≫ magnetite, 5–10:60 vol.% within oxide-rich layers) are commonly associated with apatite and rimmed by biotite (2 to 4 vol.%). Apatite prisms comprise 4 to 8 vol.%, whereas magmatic quartz (<0.5 mm) and traces of sulphides, which are generally adjacent to oxides, total <1 vol.%.

XOAGN is mineralogically very similar to the OAGN, but contains sub-rounded to rounded, 10 to 50 mm diameter, xenoliths of the country rock and oxide-rich layers are lacking. Grain size reduction, recrystallisation and rotation of plagioclase grains and country rock xenoliths have occurred and deformation is more intense compared to the other intrusive units in the intrusion. Green and brown hornblende and biotite are recrystallised and wrap around the xenolith margins, thus defining the foliation in the rock.

Structure and primary fabrics

A brief structural history of the Nebo–Babel deposit has been determined from the drill core logging. The following summary of the structural events is divided into those that have affected the country rock only and those that have also overprinted the intrusion. Primary magmatic fabric, textures, and contact relationships are also discussed.

Structure

The intensity of the gneissic foliation in the country rock ranges from preserved granitic textures through weak to moderate preferred orientation of biotite and amphibole grains, through to strong mylonitic fabric (Fig. 9a). The mylonite zones vary from several centimetres to several metres in width and are characterised by significant grain size reduction and recrystallisation. Locally, the strain intensity has resulted in ultramylonitic textures.

The degree and intensity of deformation in the country rock is not shown by the intrusion (c.f. Fig. 9d to h, with a).

Fig. 12 Detailed drill hole intersection through the upper contact at Babel (WMN 1018 drill hole) showing the sheeted nature of the contact and down-hole whole-rock Ni concentration (wt%) ▶

The most pronounced deformation in the intrusive suite is restricted to the upper intrusive contact, the apophysis at the western end of Babel, and the xenolithic OAGN south of Nebo. Mylonitic zones up to several centimetres wide, defined by grain size reduction and recrystallisation along grain margins, do occur within the gabbronorites. Brittle and, less commonly, ductile, millimetre to centimetre scale, late fault zones cross-cut all of the lithologies including the post-intrusion dykes, but do not appear to have caused any major dislocation of the intrusive units. Thus, the primary magmatic internal configuration of the intrusion is generally well preserved. However, a major N–S fault zone, the Jameson Fault, is interpreted to have transected and dislocated the originally continuous Nebo–Babel intrusion (Figs. 3 and 4).

Contact relationships

The upper and lower contacts between the country rock and the intrusion are sheeted in nature, consisting of alternating felsic orthogneiss and chilled margin apophyses, and several marginal breccia-zone lenses (MBZ; Fig. 12). The Ni wt% and sulphide % within the individual MBZ lenses (Fig. 12) are positively correlated. Thus, a MBZ lens at ~46-m depth, with high percentage of country rock xenoliths, has a low Ni wt% (Fig. 12). Multiple chilled margin dykes, up to 1-m wide, extend parallel to gneissic foliation for several tens of metres into the country rock. The degree of deformation and shearing between the country rock and the chilled margins is significantly higher along the upper contacts (Fig. 13b), with intrusive contacts generally preserved along the lower contact (Fig. 13a). Locally, sub-rounded to irregular xenoliths of orthogneiss in the chilled margins have a range of textures that indicate partial to relatively high degrees of resorption as defined by variation from irregular 1- to 3-cm-diameter xenoliths to discrete feldspar xenocrysts.

Sulphides in the upper MBZ are characterised by the most intense ductile deformation within the intrusion and locally contain folded and mylonitised orthogneiss xenoliths (Fig. 13c). Chilled margin xenoliths within massive sulphides indicate that the latter have been emplaced following crystallisation of the chilled margins. Locally, resorbed orthogneiss xenoliths in a sulphide matrix occur within the upper VLGN.

Massive sulphide veins, several tens of centimetres wide, occur in the orthogneiss up to 15 m away from the upper orthogneiss-chilled margin contact. Sulphide veins are parallel to sub-parallel to the mylonitic or gneissic fabric and contain mylonitised orthogneiss xenoliths and individual feldspar phenocrysts derived from the orthogneiss

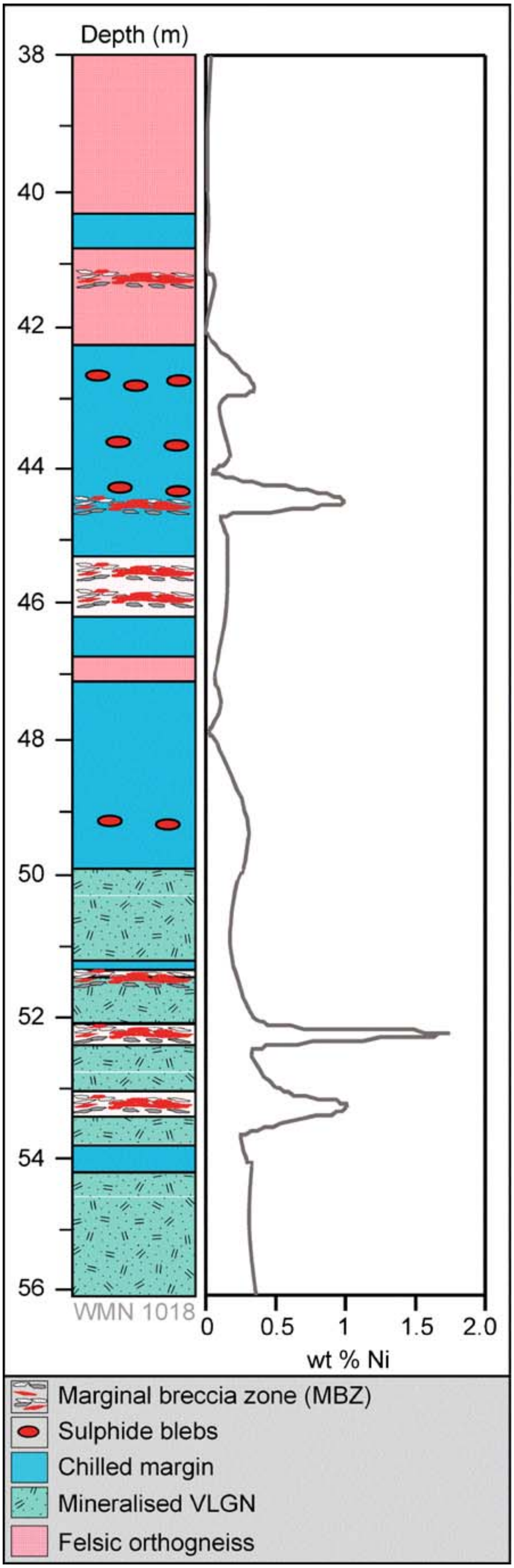

(Fig. 13d). Locally, massive sulphide veins are characterised by cuspate margins compared to the adjacent, relatively planar, mylonitic foliation (e.g. Fig. 13d). These relationships suggest that massive sulphide veins post-date the formation of the foliation in the orthogneiss and were emplaced relatively late in the structural history of the deposit.

Magmatic fabrics

The magmatic flow foliation, defined by the planar flow alignment of plagioclase, is best developed in the BGN and OAGN. The foliation is consistent in orientation over thicknesses of tens of metres, thus supporting planar, rather than turbulent, magma flow conditions during the emplacement of these units. The VLGN units generally lack this flow foliation. However, in drill hole WMN 1018 at Babel, a strong flow alignment of plagioclase phenocrysts in VLGN is truncated by the strong flow foliation in the underlying MGN (Fig. 13e). This relationship indicates that the MGN post-dates the VLGN and that at least two pulses of magma have been involved in the Nebo–Babel intrusion.

Locally, the OAGN unit contains oxide-rich (up to 60%) layers, up to 30 cm in width (Fig. 9h). The oxide-rich layers are parallel to the flow foliation fabric in the adjacent rocks and have relatively sharp, undeformed upper and gradational lower contacts, which would suggest that the sequence is overturned if these oxide-rich layers had formed through gravitational settling of oxides. However, formation of the oxide-rich layers as a result of the magma flow variations would make the contact relationships somewhat ambiguous: Thus, any younging indicators derived from them would be unreliable.

The fine-grained MGN unit locally exhibits small-scale rhythmic layers of plagioclase-bearing pyroxenite and gabbronorite. Plagioclase-bearing pyroxenite layers have sharp lower contacts and grade upwards into gabbronorite, which could suggest that the sequence is the right way up. However, if such layers have formed as a result of magma flow, the contact relationships would be ambiguous (e.g. Parsons 1987); thus, any younging directions derived from it are equivocal.

Petrographic aspects

Orthocumulates (e.g. Wager et al. 1960; Irvine 1982, and McBirney and Hunter 1995) consist of one or more cumulus minerals (or primocrysts) and new minerals crystallised from the trapped intercumulus liquid. An orthocumulate with an extreme amount of trapped liquid could show almost the whole mineralogical range of the layered intrusion within a single thin section (Cox et al. 1979) due to mineral re-equilibration as the progressive crystallisation of the trapped liquid. Methods to assess the amount of trapped liquid preserved in a rock include use of incompatible elements

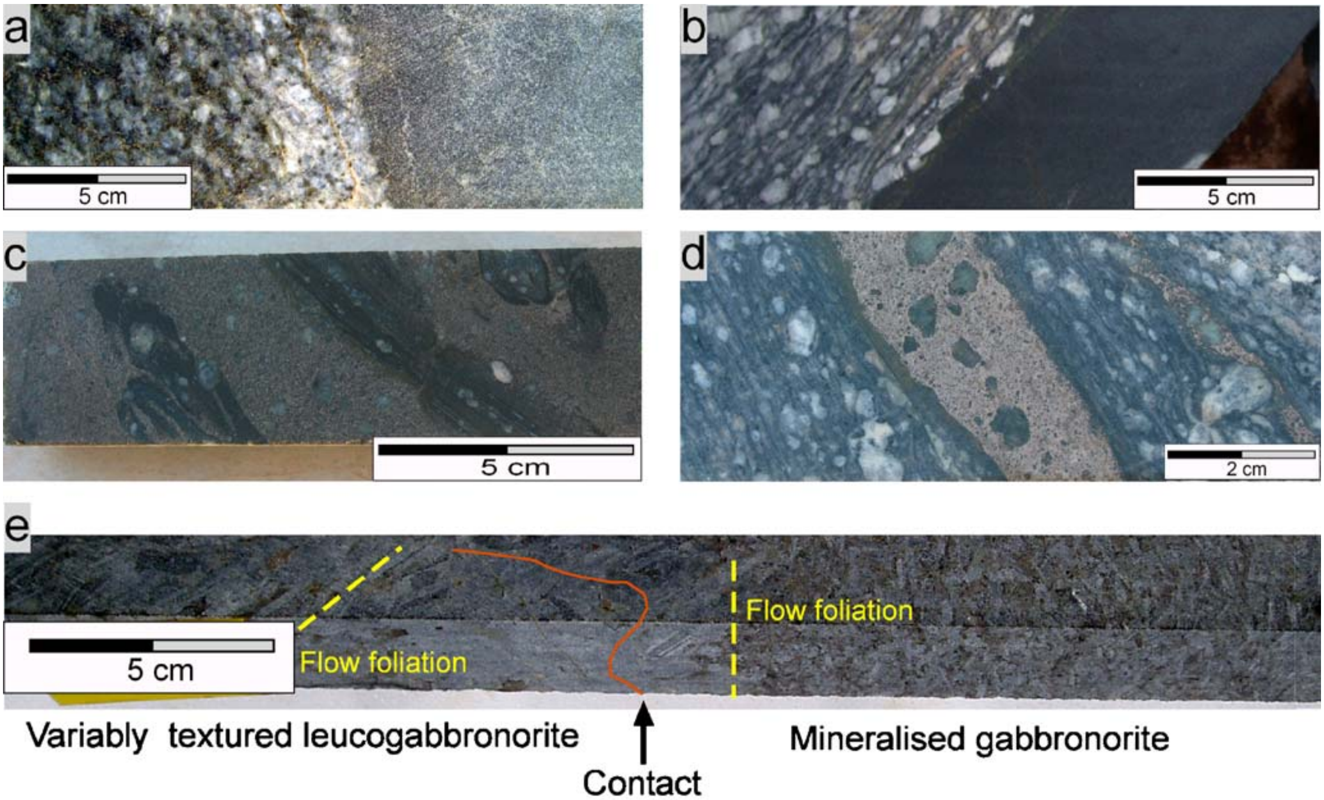

Fig. 13 Photographs showing different contact relationships between some of the different rock units in the Nebo–Babel intrusion: **a** an intrusive contact between the basal chilled margin gabbronorite and orthogneiss country rock WMN1031 677.0 m, **b** a mylonitised contact of a chilled margin apophysis WMN1031 255.2 m, **c** massive sulphide vein containing very deformed, almost ultramylonitised, and folded orthogneiss xenoliths WMN1013 122.4 m, **d** sulphide vein emplaced sub-parallel to the mylonitic foliation WMN1013 121.6 m, **e** an intrusive contact between VLGN and MGN (note that flow foliation in the VLGN terminates at the contact indicating that VLGN pre-dates MGN) WMN1018 157.5 m

such as P or U (Wager 1963; Campbell 1978), calculations based on Mg/Fe exchange between cumulus olivine or pyroxene and trapped intercumulus liquid (Barnes 1986) or combinations of the above methods (Wilson 1992). Hunter (1987) pointed out that the use of textural features to estimate the amount of trapped liquid does not account for late magmatic or post-cumulus equilibration, and in such cases, even chemical criteria can be misleading.

In addition to plagioclase and pyroxenes, gabbronorites within the Nebo–Babel deposit contain ilmenite, magnetite, apatite, biotite, hornblende, and rare zircon (c.f. Fig. 11). Plagioclase cores have wide compositional ranges ($An_{48–66}$, Figs. 14 and 15). Moreover, plagioclase crystals, even within a single thin section, are characterised by cores that are highly variable in composition and show continuous normal zoning towards rims that are up to An_{15} more sodic. Orthopyroxene has similar core–rim relationships except that the rims are more iron-rich than the cores. Based on these mineralogical and textural features, the Nebo–Babel gabbronorites are most likely to be orthocumulates, with moderate to high degrees of trapped intercumulus liquid.

Mineral chemistry

Mole percent anorthite (An) in plagioclase and 100 Mg/($Mg+Fe^{2+}$) ratio (X_{Mg}) in orthopyroxene are used to assess the degree of fractionation within and between the different units. As the main aim is to interpret the early magmatic crystallisation history of the magmatic system, the focus here is on the core compositions of the mineral grains rather than the rims. The core compositions presented are averages of more than 15 analyses per sample, with two or more spot analyses on each core. A summary of mineral compositions is provided in Table 3.

The variation in plagioclase and orthopyroxene compositions with depth at Babel is presented in Fig. 14 (drill hole WMN 1018; see Fig. 7 for drill hole location). Plagioclase An% and X_{Mg} of orthopyroxene are positively correlated, as would be expected from co-precipitation (Fig. 14; Table 3). Plagioclase has variable core compositions, although the mean values for each sample are considered representative. The most primitive plagioclase at Babel, $An_{51–77}$ (mean An_{61}), is in the VLGN, and the most evolved, $An_{46–62}$

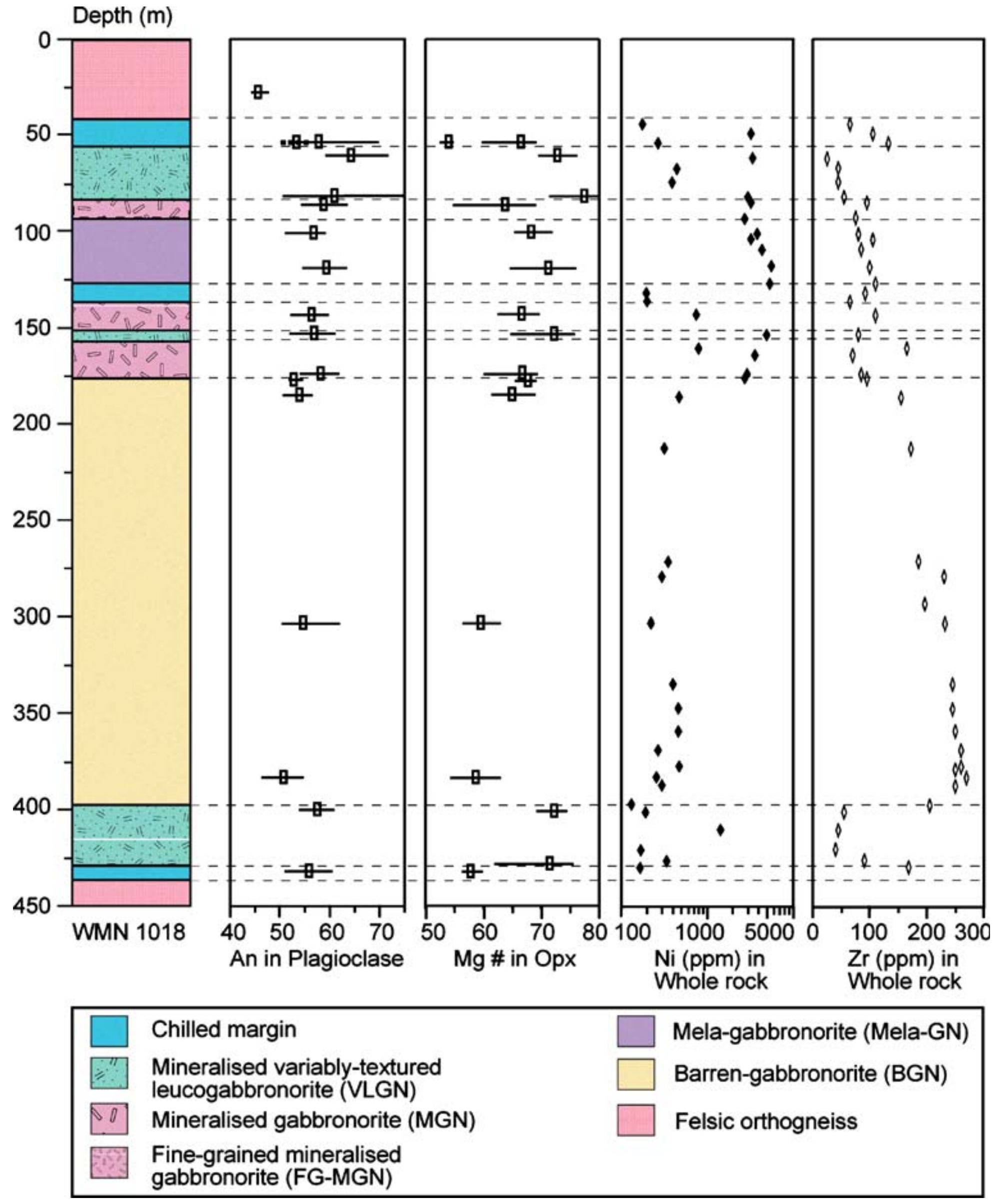

Fig. 14 Variations of plagioclase and orthopyroxene compositions, whole-rock Ni and Zr concentrations with depth in WMN1018 drill hole at Babel. *An* Anorthite, *Mg* # Mg number, *Opx* orthopyroxene

(mean An_{53}), is in the BGN (Fig. 14 and Table 3). Plagioclase An% increases upwards in the VLGN unit along the upper contact of the intrusion, but the opposite is recorded within the mela-GN (An% decreases upwards; Fig. 14). Plagioclase An content in MGN varies from 52 to 62 mol%, but does correlate with stratigraphic height (Fig. 14). Plagioclase An content in the BGN varies between 52–55 mol% at the top of the unit and decreases towards the base to 46–55 mol% (Fig. 14). The most primitive orthopyroxene at Babel, $X_{Mg55–80}$ (mean X_{Mg72}) is in the VLGN, and the most evolved $X_{Mg54–69}$ (mean X_{Mg63}) is in the BGN (Fig. 14). The X_{Mg} decreases from X_{Mg77} at the top to X_{Mg64} at the base of the VLGN unit along the top of the intrusion (Fig. 14), whereas there are only minor differences in orthopyroxene compositions within the VLGN along the base of the intrusion (Fig. 14). The X_{Mg} within the MGN and mela-GN varies from $X_{Mg60–76}$ (Fig. 14). In the BGN, it increases upwards from X_{Mg59} to X_{Mg68} (mean values; Fig. 14). Differences in An or X_{Mg} are not recorded between the MGN and BGN units, although mineral compositions in BGN and VLGN are significantly different (c.f. Fig. 14 at ~400 m down-hole depth). Olivine composition in the VLGN unit is Fo_{71}.

Figure 15 illustrates the variation of An in plagioclase and X_{Mg} in orthopyroxene for units intersected in drill hole WMN 31 within Nebo (for drill hole location, see Figs. 6 and 10). The most primitive plagioclase cores, $An_{64–71}$ (mean An_{68}), are in the VLGN, and the most evolved plagioclase, $An_{44–52}$ (mean An_{49}), is in the OAGN (Fig. 15; Table 3). The An content of plagioclase decreases downwards in the OAGN from 49–51 to 46–50 mol% (Fig. 15), but does not correlate with stratigraphic height in VLGN. The most primitive

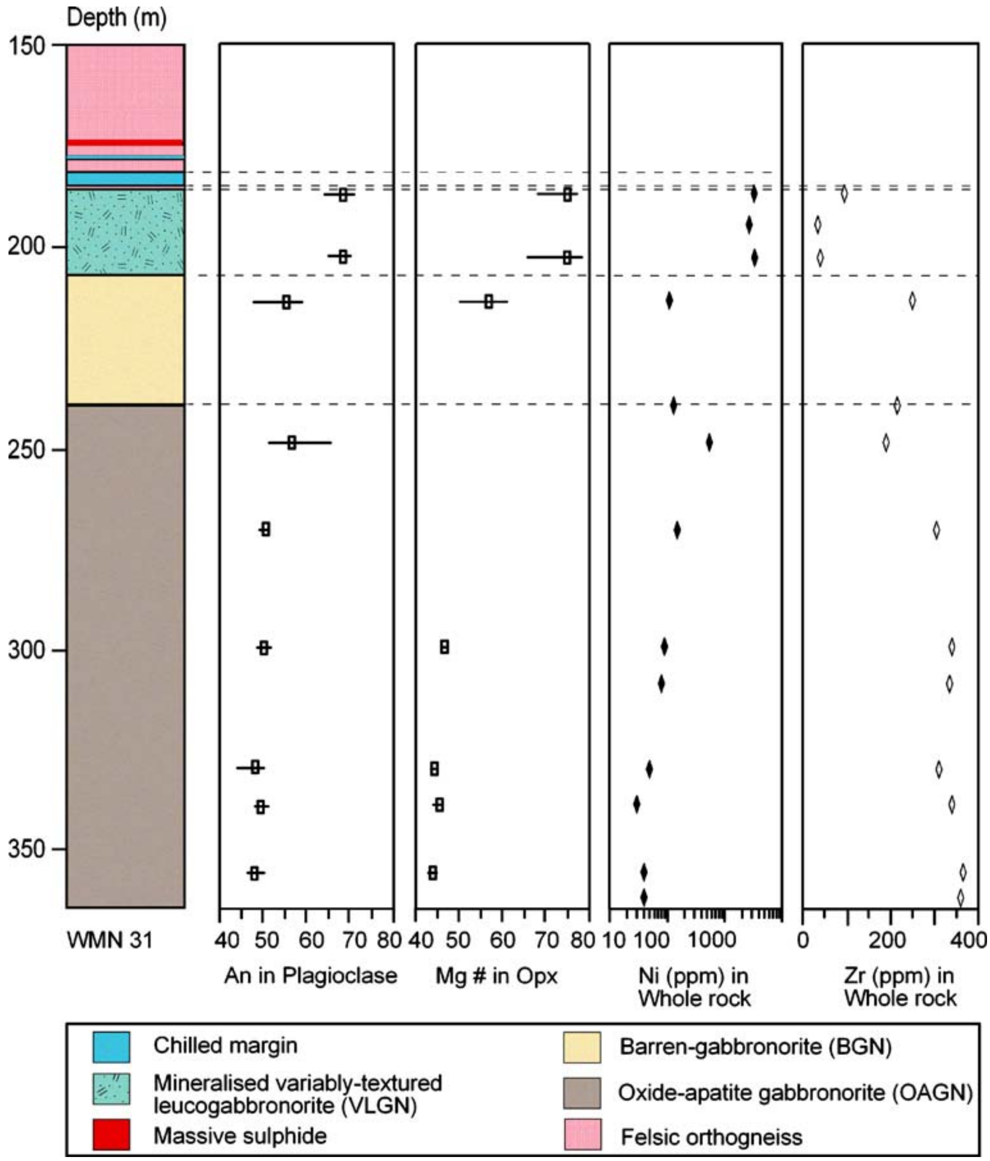

Fig. 15 Variations of plagioclase and orthopyroxene compositions, whole-rock Ni and Zr concentrations with depth in WMN 31 drill hole in the eastern part of Nebo. *An* Anorthite, *Mg #* Mg number, *Opx* orthopyroxene

orthopyroxene at Nebo, $X_{Mg66–79}$ (mean X_{Mg75}), is in the VLGN, and the most evolved $X_{Mg43–47}$ (mean X_{Mg45}) is in the OAGN (Fig. 15). Orthopyroxene in the OAGN shows a decrease downwards in the OAGN from X_{Mg47} to X_{Mg43} (Fig. 15). As at Babel, there are significant differences in plagioclase and orthopyroxene compositions between VLGN and BGN units (Fig. 15).

Whole-rock chemistry

Representative whole-rock major and trace element analyses of the major rock units within the Nebo–Babel intrusion are presented in Table 4. However, a significant proportion of the samples are sulphide-bearing, thus influencing the concentrations of other elements within those samples. The analysis totals in Table 4 are the sums of major elements as oxides and loss on ignition without S. Recalculation of the analyses to a sulphide-free basis indicates that differences are not significant enough to warrant the use of a recalculated data set.

Major elements

MgO is used as an index to measure fractionation trends within the Nebo–Babel intrusion (Fig. 16), as MgO concentrations range from ~3 wt% in the most evolved VLGN sample, with the least pyroxene, to >15 wt% in the mela-GN with approximately 50–60 vol.% pyroxene. Major element oxides, excluding Fe_2O_3, correlate negatively with MgO (Fig. 16). Conversely, Fe_2O_3 (Fig. 16) and MnO correlate positively

Table 3 Summary of plagioclase and orthopyroxene core compositions from the Nebo–Babel Intrusion

Location	Unit	An in Plag		X_{Mg} in Opx	
		Range	Mean	Range	Mean
Babel	Chilled margin	51–61	56	56–60	58
	VLGN	51–77	61	55–80	72
	MGN	52–62	57	60–76	69
	Mela-GN	51–64	58	65–76	70
	BGN	46–62	53	54–69	63
Nebo	VLGN	64–71	68	66–79	75
	BGN	48–51	56	50–61	57
	OAGN	44–52	49	43–47	45

Data plotted in Figs. 14 and 15
An Mole percent anorthite in plagioclase; X_{Mg} 100 Mg/(Mg + Fe^{2+}) in orthopyroxene

with MgO, attributed to Mn^{2+} substitution for Fe^{2+} in the pyroxene crystal structure (because this governs FeO). For a number of elements (e.g. CaO and Al_2O_3; Fig. 16), this correlation is linear, and most units, excluding OAGN, exhibit a single common trend. VLGN mostly has higher Al_2O_3 and CaO and lower Fe_2O_3, at a given MgO (Fig. 16) compared to the gabbronorite units, reflecting higher plagioclase and lower pyroxene abundance. Well-defined correlations in the CaO–MgO and Al_2O_3–MgO plots of the leuco- and gabbronorites reflect the dominance of plagioclase and pyroxenes in these units. The OAGN unit has significantly lower Al_2O_3 and higher Fe_2O_3 concentrations that reflect strong enrichment in ilmenite and magnetite (Fig. 16). However, high Fe_2O_3 concentrations (i.e. >20 wt%) in the F.G. MGN reflect high modal sulphide abundance (Fig. 16b). Major element trends for MGN and BGN overlap extensively, and thus, these units cannot be distinguished based on major element concentrations. SiO_2, TiO_2, and K_2O (not illustrated) show no correlation with MgO; however, TiO_2 can be used to distinguish between units as TiO_2 increases in the order: VLGN, MGN, and BGN with OAGN being the most enriched (Fig. 16d). Very similar trends against MgO are shown by P_2O_5 (not illustrated), which reflects progressive increase in apatite abundance. Major element concentrations in the orthogneiss country rock are significantly different compared to those of the intrusive units; for instance, MgO concentration is lower than 2 wt% (Fig. 16).

Trace elements

Trace element analyses of the Nebo–Babel units are also listed in Table 4 and are plotted using MgO as a fractionation index (Fig. 17). Chromium concentrations (<20 ppm in VLGN and OAGN units and >700 ppm in the mela-GN) correlate positively with MgO, reflecting the increase in pyroxene in the mela-GN (Fig. 17). Nickel shows a weak positive correlation with MgO in barren (i.e. <1,000 ppm Ni) gabbronorites, suggesting that, in addition to the presence of trace sulphides, it is also controlled by pyroxene (Fig. 17b). The F.G. MGN has the highest Ni content, and all mineralised units generally have Ni concentrations higher than 2,000 ppm, but exhibit considerable variations (Fig. 17b). Conversely, Cu (not illustrated) shows no systematic correlation with MgO in the barren units, but Cu and Ni trends in the mineralised units are very similar. Mineralised and barren units are clearly distinguished based on Ni concentrations, and there is significant decrease in Ni content between MGN and BGN (see Fig. 14, 175 m down-hole), but there is no overall correlation between Ni and stratigraphic height within the upper, mineralised part of the intrusion (Fig. 14). However, Ni concentrations increase towards the base within mela-GN and appear to decrease towards the base within the lower-most part of MGN (Fig. 14). There also appears to be an overall decrease in Ni concentrations from the top towards the base of the BGN at Babel, but there are no obvious differences in Ni content between the BGN and barren VLGN at the base of the intrusion (Fig. 14). Down-hole variation in Ni concentrations at Nebo is shown in Fig. 15. There is a significant change in Ni content between mineralised VLGN and BGN (Fig. 15, ~220 m down-hole). Nickel concentrations in OAGN are negatively correlated with stratigraphic height and decrease from 150 ppm at the top of the unit to 40 ppm at the base (Fig. 15), thus suggesting that the base of this unit is more evolved or contains almost no trace sulphides compared to the top (Fig. 15). Strontium has an inverse correlation with MgO (not illustrated), consistent with incompatible behavior during pyroxene fractionation. Leucogabbronorites have higher Sr concentrations compared to gabbronorites, and the mela-GN has the lowest Sr concentrations, reflecting its highest pyroxene abundances. Niobium, Zr, and Y (not illustrated) concentrations do not correlate with MgO (Figs. 14 and 17d). Niobium has a similar behaviour to

Table 4 Representative whole-rock XRF chemical data for Nebo–Babel Intrusion rocks

Sample no.	1057_003	1018_003	1018_011	1031_062	1013_064	1018_033	31_007	70_004	1018_061	1018_101	1092_025
Location	Babel	Babel	Babel	Babel	Babel	Babel	Nebo	Nebo	Babel	Babel	Babel
Drill hole	1057	1018	1018	1031	1013	1018	31	70	1018	1018	1092
Meters DH	186.9	28.1	43.9	676.4	628.0	62.0	204.0	95.6	153.6	401.0	236.8
Rock type	Orthogneiss	Orthogneiss	Chill	Chill	Micro-GN	VLGN	VLGN	Troctolite	VLGN	VLGN	VLGN
Major (wt %)											
SiO_2	66.9	60.07	47.76	48.19	50.22	48.4	46.2	46.92	47.9	51.5	50.32
TiO_2	0.66	1.28	1.26	1.53	0.47	0.30	0.27	0.24	0.52	0.49	0.62
Al_2O_3	15.4	15.80	14.56	12.71	19.81	24.3	20.4	18.42	19.4	22.4	23.06
Fe_2O_{3TOTAL}	4.36	8.19	14.77	17.03	7.77	7.51	10.2	10.03	10.6	5.81	6.41
MnO	0.11	0.22	0.23	0.23	0.12	0.07	0.09	0.12	0.1	0.09	0.09
MgO	0.54	1.22	8.12	7.86	9.49	3.91	6.51	11.99	4.7	5.01	4.99
CaO	4.26	6.40	11.49	11.02	9.26	11	9.82	9.33	10.2	10.2	11.14
Na_2O	2.82	2.83	1.46	1.51	2.41	2.84	2.47	1.93	2.97	3.24	2.94
K_2O	4.12	2.65	0.31	0.4	0.33	0.33	0.31	0.19	0.45	0.42	0.46
P_2O_5	0.352	0.92	0.08	0.07	0.08	0.048	0.083	0.08	0.176	0.14	0.13
LOI	0.22	0.06	−0.05	−0.52	−0.02	1.29	2.58	−0.37	1.6	0.39	−0.18
Total	**100.1**	**99.71**	**100.14**	**100.14**	**99.90**	**100.8**	**99.64**	**99.94**	**99.62**	**100.02**	**100.11**
Trace (ppm)											
S	410	1,300	1,500	1,200	500	16,600	23,500	11,300	23,100	450	1,900
Co	15	52	85	96	74	78	129	90	150	33	59
Cr	10	17	238	95	442	150	130	250	140	140	154
Cu	b.d.	0	187	205	61	3,350	2,930	1,870	4,130	130	58
Nb	17	19	2	3.4	1	1	1	1	4	2	3
Ni	20	1	177	151	222	3,390	3,400	1,660	4,900	190	121
Rb	114	72	4	5.2	6	15	15	3	18	12	7
Sr	337	433	204	224	295	374	321	244	304	355	351
Th	6	12	b.d.	0.7	b.d.	b.d.	b.d.	b.d.	b.d.	b.d.	b.d.
U	3	b.d.	b.d.	b.d.	b.d.	b.d.	b.d.	b.d.	b.d.	b.d.	b.d.
V	b.d	b.d.	360	410	99	50	30	52	40	50	93
Y	57	91	24	32	8	9	9	4	18	12	11
Zn	100	178	109	129	51	50	80	57	65	45	44
Zr	485	773	65	35	39	25	40	14	80	55	51

TiO_2 increasing in the order: VLGN, MGN, BGN, and the OAGN has elevated Nb (15 ppm to <30 ppm), reflecting higher oxides and apatite±zircon content (Fig. 17b,d). Down-hole Zr concentrations at Babel progressively increase from the top of the MGN towards the base of the BGN (Fig. 14). Furthermore, there is a significant change in Zr concentrations between MGN and BGN (i.e. 95 to 155 ppm Zr; Fig. 14, at ~175 m down-hole) and between BGN and VLGN (i.e. 250 to 55 ppm Zr; Fig. 14, at ~400 m down-hole), which strongly suggests multiple magma pulses rather than in situ fractionation between these units. The increase in Zr cannot be due to orthogneiss xenoliths, as none were recorded by detailed drill core logging (c.f. Fig. 17b). Zirconium concentration show progressive increase towards the base at Nebo (Fig. 15) with similar differences in concentrations between VLGN and BGN, but the trends between BGN and OAGN are continuous (Fig. 15).

To further assess the relationships between the major rock units, fractionation trends and the affects of post-magmatic alteration, plots of incompatible elements considered to be relatively immobile, such as Zr, Y, and TiO_2, are used. Yttrium (not illustrated) and Zr correlate positively with TiO_2, and the OAGN has elevated Y and Zr (Fig. 17d). Figure 17d indicates that oxides, apatite, and zircon within OAGN reflect the concentrations of TiO_2, P_2O_5, and Zr, respectively. The VLGN units are chemically uniform over the strike length of the intrusion (c.f. Figs. 14 and 15).

Chilled margins and parental magma composition

The chilled margins are considered to be much closer to the parental liquid composition than the coarser-grained gabbronorites, which are orthocumulates with variable amounts of intercumulus liquid. However, the chilled margins do not necessarily represent primitive liquid compositions because they are likely to have undergone fractional crystallisation deeper in the magmatic system and/or contamination by crustal lithologies. Nebo–Babel chilled margin rocks have more evolved mineral compositions, and generally higher incompatible element concentrations, than associated

Table 4 (continued)

1018_067	1092_004	1031_006	1031_016	1018_046	1018_051	1018_069	1018_097	70_006	70_019	31_015	31_022	32_001
Babel	Babel	Babel	Babel	Babel	Babel	Babel	Babel	Nebo	Nebo	Nebo	Nebo	Nebo
1018	1092	1031	1031	1018	1018	1018	1018	70	70	31	31	32
174.0	50.3	258.0	268.9	101.0	118.1	186.0	383.0	105.6	294.0	271.8	356.0	79.4
MGN	MGN	F.G. MGN	F.G. MGN	mela-GN	mela-GN	BGN	BGN	BGN	BGN	OAGN	OAGN	XOAGN
Major (wt %)												
48.6	49.01	41.01	44.23	46.9	47.4	50.3	49.71	47.97	50.22	41.5	41.2	44.87
0.61	0.62	1.40	0.78	0.74	0.84	0.99	1.78	1.23	1.17	5.31	4.94	3.94
16	13.24	13.52	13.74	11.6	12.8	15.2	14.26	14.61	11.11	9.97	10.5	11.85
12.2	15.05	24.99	21.55	17.6	16.7	11.3	13.68	15.44	12.95	20.9	22.1	20.67
0.16	0.21	0.2	0.29	0.23	0.2	0.19	0.21	0.19	0.25	0.3	0.33	0.3
8.01	11.47	6.3	6.57	11.4	12	8.35	8.24	7.21	9.11	6.21	5.69	3.76
9.96	8.01	8.19	8.98	7.19	6.8	9.68	9.08	8.64	12.75	9.33	9.99	8.79
2.28	1.76	1.75	2.02	1.71	1.84	2.41	2.27	2.26	1.80	1.92	2	2.25
0.35	0.31	0.5	0.47	0.35	0.38	0.5	0.69	0.68	0.48	0.77	0.79	1.41
0.201	0.19	0.47	0.35	0.174	0.245	0.404	0.39	0.47	0.50	3.13	3.41	2.59
0.62	−1.32	−3.8	−3.26	0.89	0.78	0.46	−0.39	−0.79	−0.39	−0.01	−0.66	−0.11
99.64	**99.72**	**99.47**	**99.59**	**99.78**	**100.9**	**99.99**	**100.13**	**99.94**	**100.12**	**99.56**	**100.5**	**100.01**
Trace (ppm)												
16,000	14,900	57,000	46,800	24,400	24,400	3,590	2,600	24,600	2,800	3,440	1,820	2,200
120	132	90	169	180	207	69	73	59	76	102	99	69
220	652	137	146	350	460	230	180	197	115	140	b.d.	86
2,740	120	9,440	5,280	5,030	2,480	500	270	4,160	78	100	60	33
2	2	5	2	2	4	6	10	8	6	17	19	29
2,880	2,370	6,290	6,160	3,840	5,540	470	255	1,760	133	150	40	b.d.
15	5	12	6	9	15	18	18	19	15	42	39	44
248	191	223	235	177	192	240	231	233	178	219	248	263
b.d.	b.d.	b.d.	b.d.	b.d.	b.d.	b.d.	3	3	b.d.	b.d.	b.d.	7
b.d.	b.d.	b.d.	b.d.	b.d.	b.d.	b.d.	b.d.	b.d.	b.d.	b.d.	b.d.	3
60	110	156	72	80	80	50	123	113	141	b.d.	b.d.	86
18	13	23	22	24	24	27	33	31	38	75	99	108
85	99	185	167	125	100	85	99	116	87	180	185	27
85	70	162	68	80	100	155	269	248	213	305	365	789

BGN Barren gabbronorite; *F.G. MGN* fine-grained mineralised gabbronorite; *GN* gabbronorite; *mela-GN* mela-gabbronorite; *MGN* mineralised gabbronorite; *OAGN* oxide–apatite gabbronorite; *VLGN* variably textured leucogabbronorite; *XOAGN* xenolithic oxide–apatite gabbronorite; *b.d.* below detection; *DH* down hole; *LOI* loss on ignition

VLGN units. Major element concentrations of the chilled margins are broadly similar to the BGN, but their incompatible element concentrations are generally significantly lower. The chilled margins, in the Nebo–Babel intrusive system, are closely related to the other units and are thus considered representative of the parental magma. At the pressures estimated by Ballhaus and Berry (1991), the Giles Complex parental liquids would have undergone significant orthopyroxene fractionation at the expense of olivine; consequently, these liquids were not in equilibrium with mantle compositions.

The compositions of the Nebo–Babel chilled margins are SiO_2 (48–50 wt%), MgO (8–9 wt%), Al_2O_3 (13–15 wt%), Fe_2O_{3TOTAL} (13–17 wt%), TiO_2 (0.7–1.5 wt%), S (700–1,500 ppm), and Ni (150–180 ppm). On a total alkalis–silica nomenclature diagram the chilled margins plot within the subalkaline or tholeiite field (MacDonald 1968, Fig. 18), samples plotting outside of this field are likely to be affected by lower SiO_2 concentrations related to the presence of oxides and sulphides (Fig. 18).

Mineralisation

The sulphide mineralisation in the Nebo–Babel system occurs in two main styles: massive sulphides (and associated massive sulphide breccias and stringers) and disseminated gabbronorite-hosted sulphides. Preliminary resource estimates based on 90 drill holes yield 392 million tonnes at 0.30% Ni and 0.33% Cu at a cut-off of 0.2% Ni, with a total inventory of 1.2 million tonnes of Ni metal and 1.3 million tonnes of Cu metal (Grant Samuel, WMC Resources, December 2004). Approximately 70% of the resource is in the Babel deposit.

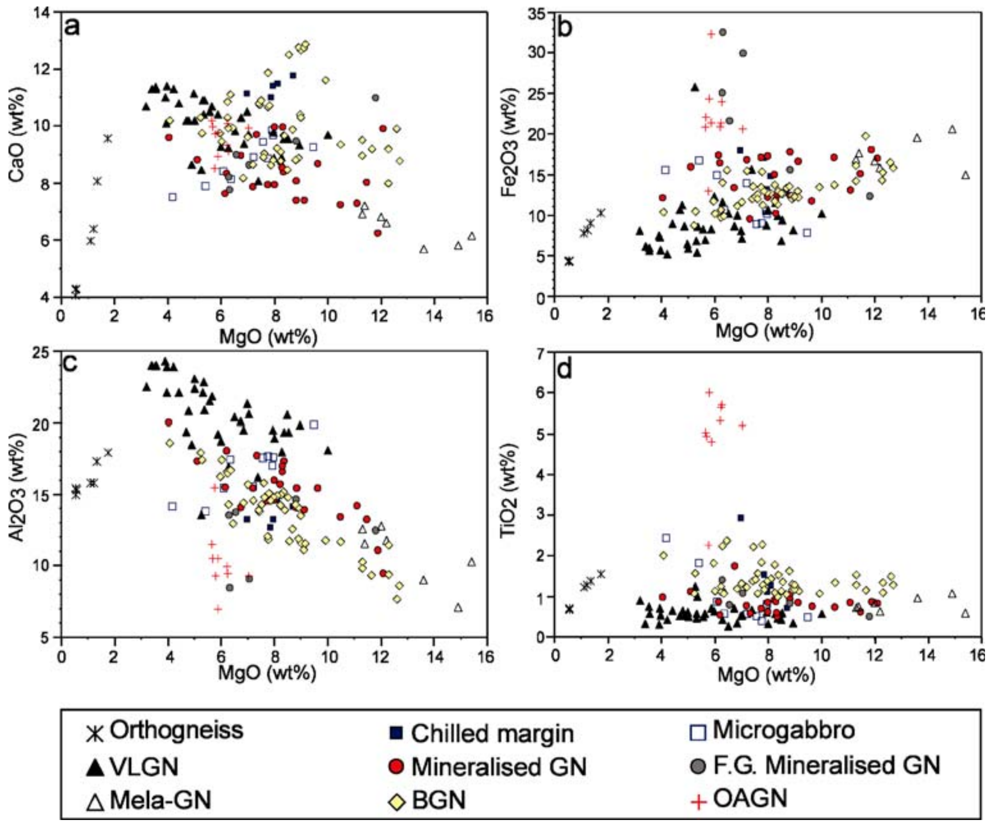

Fig. 16 Plots of MgO vs major element oxides for the Nebo–Babel intrusion

Massive and breccia sulphides

Massive and breccia sulphides, a comparatively minor component of the sulphide inventory of the deposit, are present in both Babel and Nebo deposits and are localised in pods close to, or along, the hanging wall contact with the felsic orthogneiss country rock. These sulphides are dominated by monoclinic pyrrhotite, with subordinate pentlandite, chalcopyrite, and pyrite. The average massive-sulphide Ni and Cu tenor (Ni and Cu concentration in 100 wt% sulphides) at Babel is 7.6% Ni and 0.7% Cu, whereas at Nebo, it is 5.8% Ni and 1.6% Cu. Pentlandite forms both coarse segregations nucleated on pyrrhotite grain boundaries (Fig. 19a) and low-temperature 1–50 μm exsolution flames within pyrrhotite. Chalcopyrite occurs as 100–300 μm anhedral bodies and, rarely, as coarse lamellae in pyrrhotite. No pyrrhotite-bearing samples tested with a suspension of synthetic colloidal magnetite in water (method of Soffel 1991) contained hexagonal pyrrhotite. Hypogene pyrite occurs in one massive sulphide sample in the form of plate-like bodies 8–10 mm long and 1 mm wide. In most of the shallower intersections, supergene alteration has modified the primary sulphide assemblages, with pentlandite partly altered to secondary violarite, and pyrrhotite partially altered to a phase along the greigite–violarite join, in comb-like fringes which nucleate on grain boundaries and fractures within the pyrrhotite (Fig. 19b).

Table 5 Representative whole-rock analyses of massive sulphides and mineralised gabbronorite samples from the Nebo–Babel Intrusion

Sample No.	Style	Unit	Ni (%)	Cu (%)	Zn (ppm)	S (%)	Ir (ppb)	Ru (ppb)	Rh (ppb)	Pt (ppb)	Pd (ppb)	Au (ppb)
1031–026	Massive	Mass. sulf.	7.26	0.25	14	32.1	96	238	122	23	150	10
1092–010	Dissem.	MGN	0.64	0.20	24	4.14	4	8	8	97	147	43
1031–006	Blebby	F.G. MGN	0.63	0.94	109	5.70	2	3	2	63	60	33
1018–061	Dissem.	VLGN	0.36	0.33	25	2.31	11	22	16	242	197	91
31–004	Dissem.	VLGN	0.33	0.40	43	2.22	3	6	4	88	112	95
70–004	Dissem.	Troctolite	0.17	0.19	35	1.13	2	5	3	45	48	41

F.G. MGN Fine-grained mineralised gabbronorite; *MGN* mineralised gabbronorite; *VLGN* variably textured leucogabbronorite

Fig. 17 Plots of MgO vs selected trace elements and Ti_2O versus Zr for the Nebo–Babel intrusion

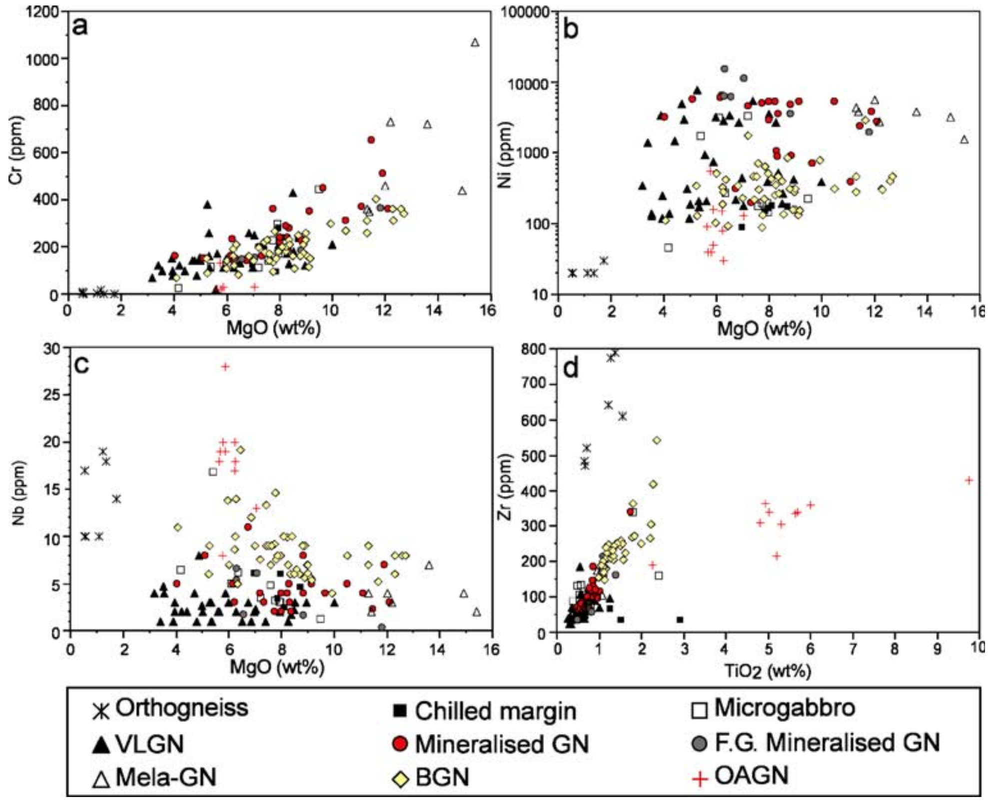

Disseminated sulphides

Most mineralisation in the two deposits is in the form of disseminated blebs in gabbronorite. The main host units are the MGN, F.G. MGN, VLGN along the upper contact, and mela-GN with disseminated sulphide mineralisation also present in minor troctolite bodies. The average tenor of disseminated sulphides at Babel is 5.6% Ni and 7.0% Cu, whereas it is 5.5% Ni and 6.9% Cu at Nebo. The disseminated sulphides occur as bleb-like aggregates or as sulphide blebs (50 μm to 12 mm), which tend to form angular blocks and thin laths at interstices between blocky pyroxene and plagioclase crystals.

Phase mineralogy and micro-textures are essentially identical to those in the massive sulphide bodies, except that pentlandite tends to be concentrated on the margins of the blebs (Fig. 19c). Trace quantities of other sulphides, such as bornite, sphalerite and galena, and tellurides, altaite and melonite, are detected with SEM, but are rarely coarse-grained enough to be identified using optical microscopy. Chalcopyrite appears to have been particularly susceptible to post-crystallisation textural modification and grain-scale remobilisation and forms a network of microveinlets in fractured plagioclase in places (Fig. 19d). It is suggested that the fracturing of plagioclase and subsequent remobilisation of chalcopyrite results from volume expansion of adjacent pyroxenes during their partial uralitisation. Rare hypogene pyrite tends to occur as 100–600 μm cauliflower-like or roughly cubic crystals embedded in other sulphides. Some supergene alteration occurs as in the massive sulphides.

Sulphide mineral chemistry

The mineral compositions of the individual sulphide phases in the Nebo–Babel system are consistent with the established phase relations for a monoclinic pyrrhotite–pentlandite–chalcopyrite assemblage (see Misra and Fleet 1973).

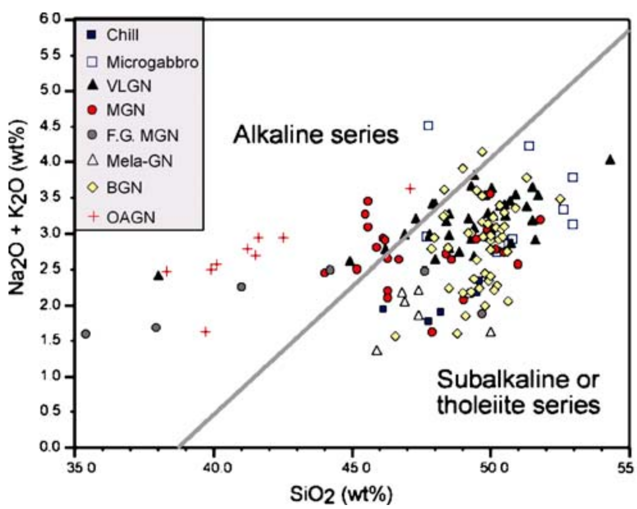

Fig. 18 Alkaline and subalkaline (tholeiitic) subdivision on a total alkalis–silica diagram (subdivision boundary from MacDonald 1968)

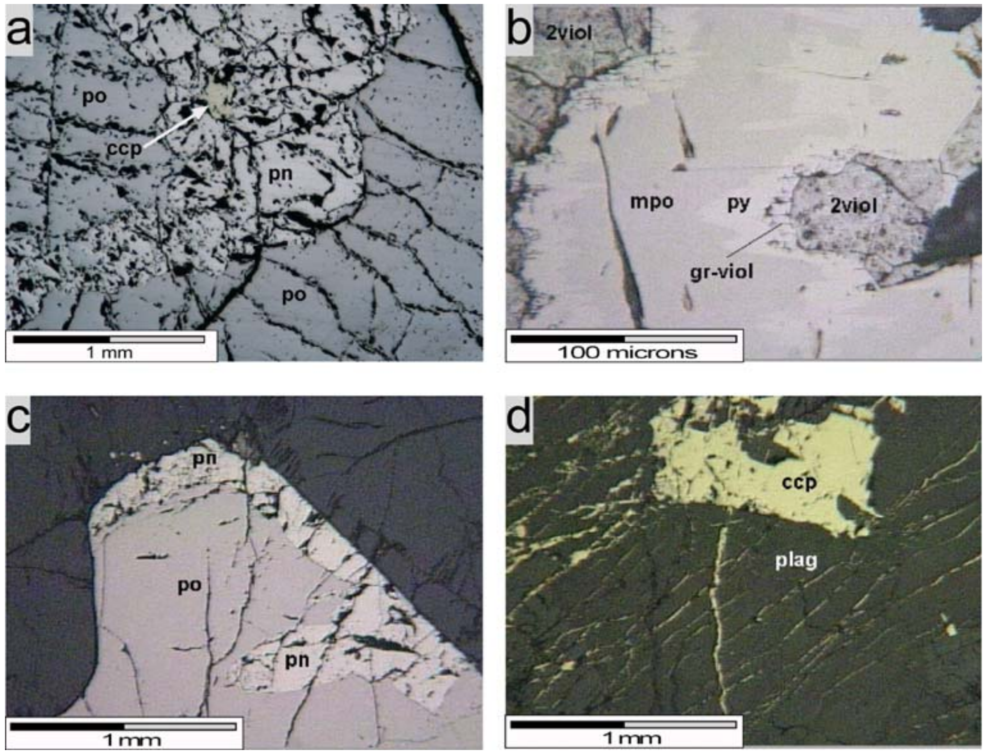

Fig. 19 Photomicrographs (*reflected light*) of mineralogical and textural relationships of sulphides in the Nebo–Babel deposit: **a** pentlandite segregation in massive sulphide, with minor chalcopyrite, WMN1031 289.3 m, **b** detail of transition zone assemblages, porous secondary violarite (*2viol*) after pentlandite, is bordered by a thin fringe of a phase on the violarite–griegite join (*gr–viol*). This is preceded by a coarser fringe of nickeloan pyrite (*py*). Relict unaltered pyrrhotite (*mpo*) in the centre, WMN1030 51.6 m, **c** pentlandite segregation (*pn*) on the grain margin of a pyrrhotite-rich bleb (*po*). Dark minerals are silicates, WMN1092 88.8 m, **d** fine microveinlets of chalcopyrite infilling fractures in plagioclase (*plag*). A coarser segregation of chalcopyrite (*ccp*) is also present, WMN1013 136.4 m. *ccp* Chalcopyrite, *gr* griegite, *plag* plagioclase, *pn* pentlandite, *po* pyrrhotite, *py* pyrite, *viol* violarite

The Ni and Co contents of pentlandite in this assemblage are more or less constant and centre on 36 and 1.2 wt%, respectively. The Ni content of monoclinic pyrrhotite varies from 0.10 to 1.25 wt% with a mean of 0.61 wt% (258 analyses). Chalcopyrite is essentially stoichiometric. Hypogene pyrite is low in Ni (0.02–0.20 wt%) but locally Co-

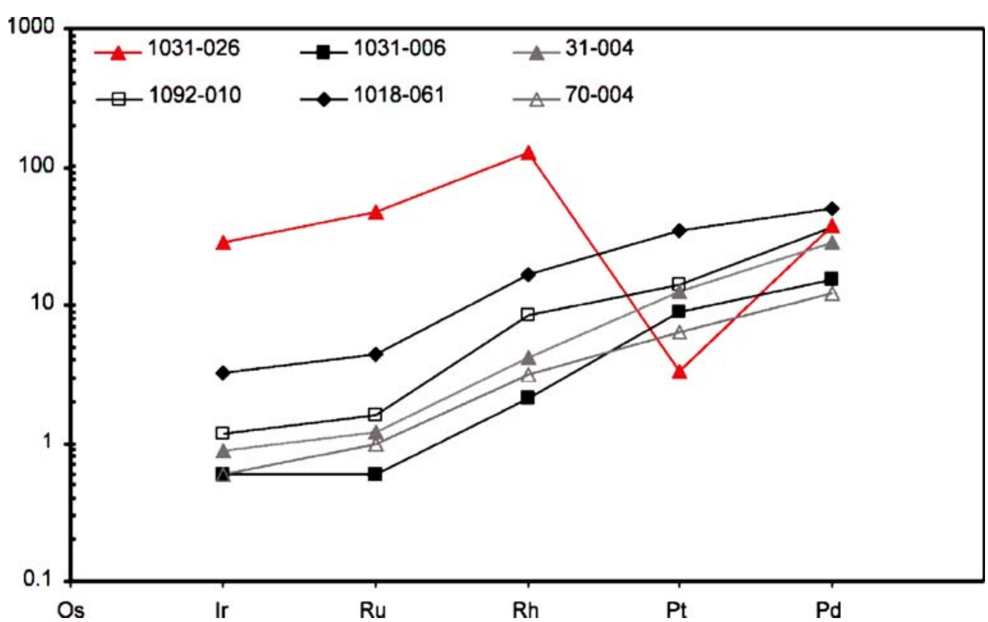

Fig. 20 Primitive mantle-normalised plots of the representative massive and disseminated sulphides at the Nebo–Babel deposit (normalisation factors from Barnes and Maier 1999)

rich (up to 3.40 wt%). Conversely, supergene pyrite is Ni rich (0.50–6.80 wt%) and Co poor (<0.07 wt%), reflecting a pyrrhotite precursor. The majority of analyses of supergene violarite-type phases plot roughly mid-way between end-member violarite and greigite, with four samples plotting near the violarite end of the violarite–polydymite join. The latter represents violarite replacements of pentlandite rather than pyrrhotite.

PGE contents and mineralogy

Representative PGE analyses of the Nebo–Babel massive and disseminated sulphide samples are presented in Table 5. Combined PGE contents of disseminated sulphide samples range between 103 and 488 ppb with Pt and Pd predominating. Two massive sulphide samples from Babel were analysed and show significantly different PGE geochemistry to the disseminated samples. Total PGE contents (exclusive of Os) for the two massive sulphide samples are 798 and 628 ppb, respectively, and Ni/PGE ratios are very high (60,000–116,000), relative to the disseminated mineralisation (7,300–24,000). This, and the fact that the massive sulphides have significantly higher relative IPGE (Ru, Os, and Ir, Barnes et al. 1985) levels (Fig. 20), suggests either a different source for the massive sulphides or, more likely, that the massive sulphide component has undergone sulphide-melt fractionation (e.g. Barnes and Maier 1999).

Samples of mineralised material scanned in an SEM in backscattered mode contain moncheite ($PtTe_2$), merenskyite ($PdTe_2$), and michenerite (PdBiTe), together with melonite ($NiTe_2$) with significant Pd substituting for Ni. These minerals are typically anhedral grains (1 to 4 μm, rarely up to 10 μm) hosted in pyroxenes, plagioclase, pyrrhotite, K-feldspar, and quartz.

Discussion

To date, the Nebo–Babel Ni–Cu–PGE deposit is the most significant nickel sulphide discovery associated with the, approximately, 1,078-Ma Giles Complex and Warakurna LIP in central Australia. The large, low-grade deposit is associated with the low-MgO, relatively evolved, essentially olivine-free, gabbronorite intrusion emplaced in sulphide-free amphibolite-facies granitic gneiss. The deposit is hosted in a magma chonolith, which is defined as an igneous intrusion whose form is so irregular that it cannot be classified as a laccolith, dyke, sill, or other recognised body (Bates and Jackson 1987). It has several similar geological features to other world-class Ni–Cu sulphide deposits, for example, Jinchuan, China, Noril'sk, Russia, Voisey's Bay, Canada, and Uitkomst, South Africa, which all occur in magma conduit systems (Naldrett 1999).

The Nebo–Babel deposit occurs within a relatively small, open system, tube-like intrusion (5×1×0.5 km), which is comparable in size and morphology to those at the Noril'sk deposits (e.g. Lightfoot and Naldrett 1994). These are hosted within elongate bodies (15×2×0.2 km), along which, magma has flowed en route to the overlying volcanic sequence. They also resemble the 30- to 100-m-thick feeder troctolite sheet at the Voisey's Bay deposit (Li and Naldrett 1999). Mineralogical, trace element and isotope studies at both Noril'sk and Voisey's Bay indicate that the intrusive sequence has formed through the emplacement of multiple magma pulses (e.g. Naldrett 1999 and references therein), and multiple magma pulses are also recognised within the Nebo–Babel intrusion based on the evidence presented herein. Trace element and isotope studies at both Noril'sk (e.g. Lightfoot and Naldrett 1994) and Voisey's Bay (Li and Naldrett 2000) indicate that the magmas interacted with S-bearing country rocks, thus extracting SiO_2 and S, which led to sulphide saturation of a magma. Data from this study suggest only limited interaction between the adjacent country rocks and the Nebo–Babel magmas. A significant difference however is that S-bearing country rocks, which are common feature of all world-class Ni–Cu deposits (e.g. Noril'sk and Voisey's Bay), are lacking at the Nebo–Babel. Furthermore, the Nebo–Babel deposit is associated with a significantly more evolved gabbronorite intrusion compared to the troctolite suite at the Voisey's Bay (Li and Naldrett 1999).

Fractional crystallisation

On the basis of mineralogical, textural, and chemical data, gabbronorites at Nebo–Babel are orthocumulates. The systematic variations in mineral compositions (Figs. 14 and 15) indicate that the intrusive units become progressively more evolved in the order: VLGN, MGN, BGN, and OAGN. Mineral compositions within the BGN and OAGN units show a relatively small range in compositions, but exhibit clear trends that indicate increasing fractionation towards the base of both units.

Incompatible trace-element concentrations of Y, Nb, and Zr (Fig. 17) show that there is a progression from least-evolved VLGN through MGN, to BGN and most evolved OAGN in agreement with the mineral composition trends. The most primitive mineral compositions within VLGN units suggest that they have crystallised from more primitive, but chemically similar, basic magma to the other Nebo–Babel units.

There is a successive increase towards the base in the concentrations of incompatible trace elements, such as Zr (Figs. 14 and 15), and other elements, such as Ti, P, and Nb (not shown), from upper VLGN through MGN and BGN before a sharp decrease in the lower VLGN (Fig. 14). Three possible models to explain this trend of increasing concentration of incompatible trace elements towards the base are evaluated below.

1. Progressive increase in the percentage of trapped liquid towards the base of the BGN and OAGN. Reaction between early precipitated orthopyroxene with coexisting trapped intercumulus liquid in an orthocumulate rock causes orthopyroxene re-equilibration to a more iron-rich composition, i.e. trapped liquid shift (Barnes 1986). In the BGN unit at Babel, orthopyroxene X_{Mg} decreases from X_{Mg65} at the top of the unit to X_{Mg59} at the base (Fig. 14). Using calculations from Barnes (1986), the percentage of trapped liquid required to cause this X_{Mg} displacement in BGN is ~20%. In the same stratigraphic section however, whole-rock Zr concentrations, which are inversely correlated with X_{Mg}, vary from 155 to 265 ppm (Fig. 14), i.e. an increase of 110 ppm. To account for both mineral and chemical trends, the trapped liquid must have contained 550 ppm Zr. We consider such a highly evolved liquid to be an unrealistic parental liquid to the gabbronorites, e.g. BGN at Babel. Moreover, on the basis of modal proportions of accessory mineral phases such as biotite or quartz, petrographic observations, and the degree of mineral zoning in plagioclase and orthopyroxene (c.f. Fig. 14), there is no evidence for significant variation in percentages of trapped liquid within BGN at Babel. Consequently, progressive increase in the percentage of the trapped liquid downwards towards the base of the BGN and the associated trapped liquid shift cannot account for the mineral and chemical trends observed in the Nebo–Babel intrusion.
2. Reverse crystal fractionation. Reverse crystal fractionation (e.g. Cox et al. 1979) could produce the observed mineral and geochemical trends in the BGN and OAGN units (Figs. 14 and 15). This process has been documented on a scale of several hundred metres in other layered intrusions, for example in the Stillwater Complex (Raedeke and McCallum 1984), but in all of the reported cases, reverse crystal fractionation is attributed either to a trapped liquid shift (e.g. Barnes 1986; Raedeke and McCallum 1984) or magma mixing (e.g. Mathison 1987). However, as argued above, trapped liquid shift cannot account for the mineral and chemical trends observed in the Nebo–Babel intrusion, and there is no evidence for magma mixing, and the remarkable consistency in the mineral and chemical trends within the BGN and OAGN for considerable thickness (Figs. 14 and 15) implies closed system fractionation and strongly argues against injection of magma during crystallisation of those units. Note that sharp contrasts in concentrations of incompatible trace elements such as Zr between basal VLGN and BGN (Fig. 14) cannot be produced through in situ crystal fractionation, which implies multiple magma pulses for these units. Therefore, we feel that reverse crystal fractionation or magma mixing is unlikely to have produced the observed mineral and chemical trends over such distances in the Nebo–Babel intrusion.
3. Normal crystal fractionation and overturning of the intrusion. Studies of layered intrusions (e.g. Skaergaard, Brown 1957) indicate that closed system crystal fractionation results in progressively more evolved mineral compositions towards the top of the intrusion and a concomitant increase in the whole-rock incompatible trace elements such as Zr (e.g. Great Dyke, Wilson 1992). Post-magmatic overturning would therefore result in an apparent reverse fractionation trend in such intrusions. In the Nebo–Babel intrusion, plagioclase and orthopyroxene become systematically more evolved towards the base of the BGN at Babel (Fig. 14) and OAGN at Nebo (Fig. 15) with a concomitant systematic increase in the whole-rock incompatible trace element concentrations with depth (Figs. 14 and 15). These chemical trends for both mineral compositions and whole-rock incompatible trace elements are consistent with normal crystal fractionation processes except that they are reversed. In West Musgrave, there have been two orogenic events in the past 1,200 Ma, and basic volcanic rocks (e.g. Tollu) outcrop adjacent to comagmatic, deep crustal, gabbroic intrusions (e.g. Blackstone Range; e.g. Glikson et al. 1996; Fig. 2). Therefore, it is not unreasonable to propose that structural overturning of the Nebo–Babel intrusion has taken place. Although there is no significant intrusion-scale deformation, it is likely that the structures responsible for overturning of the Nebo–Babel intrusion were of a significantly larger scale than that of the deposit. In short, there is currently no conclusive geological evidence either for or against structural overturning; therefore, we are unable to state with certainty that overturning has occurred, merely that this model seems better suited to the mineralogical and whole-rock chemical data presented here.

Emplacement model

On the basis of field, mineralogical, geochemical, and primary architectural evidence, the Nebo and Babel intrusion represents an originally continuous magma cho-

Fig. 21 Schematic cross-section emplacement model for the Nebo–Babel intrusion. Note in *Stage (iv)*, the intrusion is structurally overturned. Not to scale, flow direction due east into the page ▶

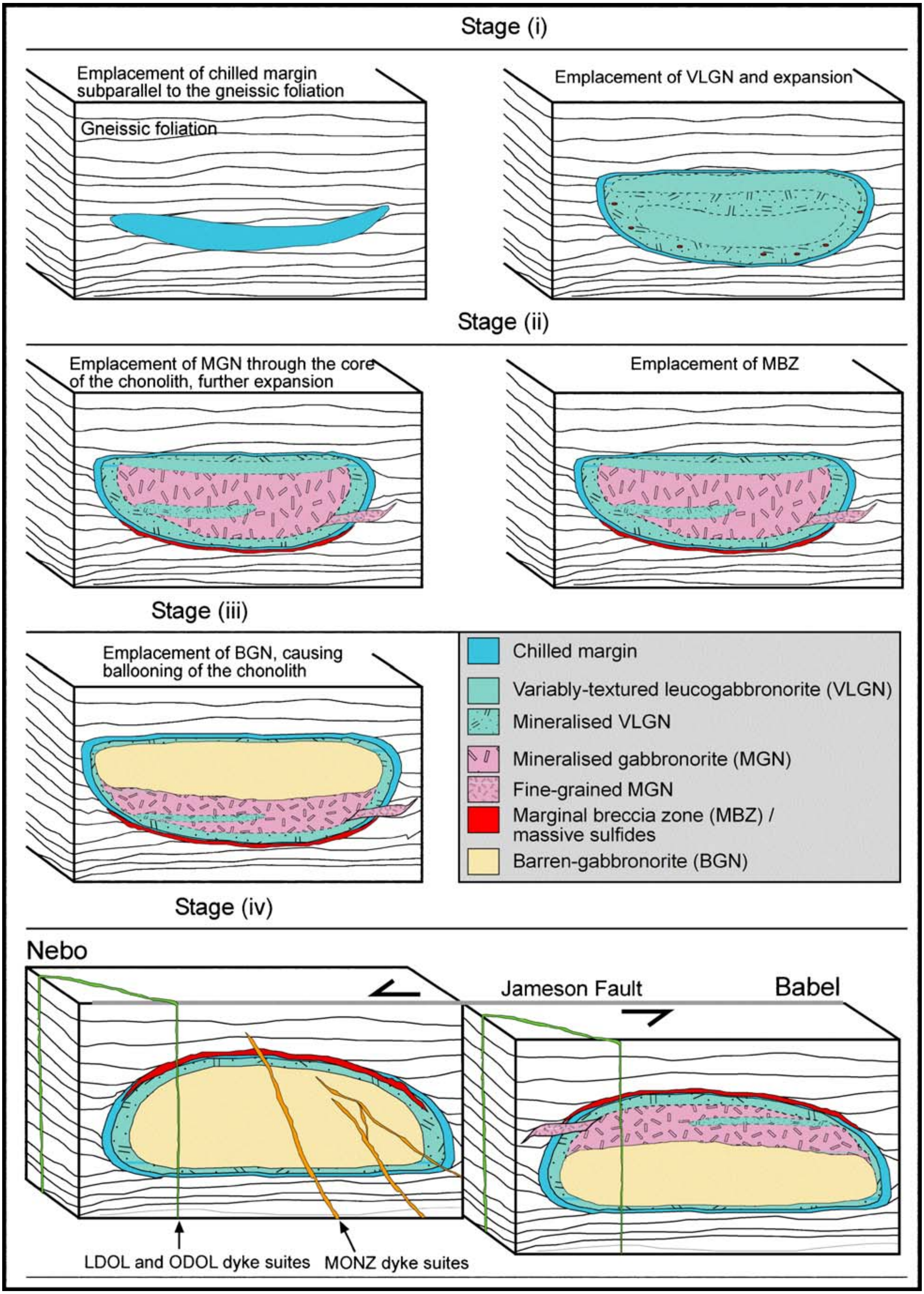
Stage (i)
Emplacement of chilled margin subparallel to the gneissic foliation
Gneissic foliation
Emplacement of VLGN and expansion
Stage (ii)
Emplacement of MGN through the core of the chonolith, further expansion
Emplacement of MBZ
Stage (iii)
Emplacement of BGN, causing ballooning of the chonolith
Chilled margin
Variably-textured leucogabbronorite (VLGN)
Mineralised VLGN
Mineralised gabbronorite (MGN)
Fine-grained MGN
Marginal breccia zone (MBZ) / massive sulfides
Barren-gabbronorite (BGN)
Stage (iv)
Nebo
Jameson Fault
Babel
LDOL and ODOL dyke suites
MONZ dyke suites

nolith. The initial magma that formed the Nebo–Babel intrusion most likely exploited a linear weakness in the country rock, such as a shear or fault zone sub-parallel or parallel to the gneissic foliation. The first stage in the formation of the intrusion involved emplacement of the chilled margin and VLGN units (Fig. 21, stage i). The occurrence of the VLGN units at the margins of the intrusion, progressive coarsening of chilled margins inwards into the VLGN and chilled margin xenoliths with the VLGN units, are all compatible with emplacement of the VLGN units first. A constant and relatively primitive composition of VLGN over a strike length of more than 5 km strongly suggests that the VLGN was emplaced under open system conditions. Furthermore, sulphide blebs in both the chilled margins and VLGN units indicate that these dynamic magma pulse(s) carried sulphides and, thus, were sulphide over-saturated.

After emplacement of the VLGN unit, a marginally more fractionated MGN unit was injected into the hotter and thermally insulated core of the intrusion (Fig. 21, stage ii), thus breaking up the existing VLGN. The emplacement of the MGN resulted in further inflation of the conduit. Mela-GN and fine-grained MGN are thought to be contemporaneous with the MGN based on transitional contacts and mineralogical and chemical similarities. This magma was also likely to have been sulphide over-saturated, based on the occurrences of sulphide blebs in the fine-grained MGN. The emplacement of MBZ could have occurred either at this or a later stage during the emplacement of BGN.

After the emplacement of the MGN unit, another pulse of fresh and more fractionated magma was emplaced between the MGN and VLGN, thus forming the BGN (Fig. 21, stage iii). After the magma flow ceased, closed system crystal fractionation of the BGN produced the observed mineral and chemical trends (e.g. Figs. 14 and 15). Magma flow was from the southwest, because MGN thickness progressively decreases towards the east, and the units in the core of the intrusion become progressively more evolved eastwards. After crystallisation, the intrusion was cross-cut by dyke suites, overturned and overprinted by post-magmatic deformation, including offset by the Jameson Fault (Fig. 21, stage iv). Architectural, mineralogical, and geochemical evidence all confirm the existence of a continuous intrusion before faulting. However, as we have argued above, there is a necessity for overturning to explain the chemical differentiation of the intrusion if normal fractionation processes are assumed to have taken place.

Ore genesis

The disseminated and massive sulphides in the Nebo–Babel deposit are restricted to the early, more primitive, and laterally chemically uniform pulses of VLGN and MGN. The spatial restriction of sulphides predominantly to margin of the deposit suggests the possibility that sulphide saturation involved reactions with the country rocks. However, this interpretation should be viewed with some caution, as the predominant occurrence of the MBZ along the top of the deposit could be partly a factor of drilling density, as relatively few drill holes intersect the basal contact at Babel (e.g. Fig. 3b), and only one drill hole penetrates the basal contact at Nebo.

Significant contamination of basic magma with crustal sulphide- or sulfate-bearing country rocks can lead to sulphide over-saturation (Li and Naldrett 1993). Liberation of S from pyrite-bearing country rocks in response to contact metamorphism can also result in S transfer into the magma and, thus, cause sulphide over-saturation (Ripley and Alawi 1993). The country rocks at the top and bottom of the intrusion and in the region generally, however, are homogeneous and sulphide-free, and sulphide-bearing country rock lithologies are extremely rare in the West Musgrave Block (Daniels 1974; Glikson et al. 1995). Therefore, it is unlikely that local crustal assimilation is important, although earlier assimilation in a deeper part of the magmatic system cannot be excluded.

Fractional crystallisation of a sulphide liquid can produce an Fe-rich cumulate enriched in Os, Ir, Ru, and Rh and a Cu-rich, more fractionated liquid, that is enriched in Ag, Au, Pt, and Pd (Barnes and Maier 1999). Significantly different PGE chemistry and Cu tenor between massive and disseminated sulphides (Fig. 20) strongly suggests that the former have undergone sulphide-melt fractionation (e.g. Barnes and Maier 1999). Moreover, contact relationships indicate that massive sulphides are late in the sequence of emplacement events. The MBZ appears to be of intrusive origin and could have formed through the emplacement of massive sulphides, either as a sulphide liquid or monosulphide solid solution, preferentially along an already significantly deformed contact of the intrusion. Partial resorption of orthogneiss xenoliths in the MBZ indicates that they have reacted with the massive sulphides. At present, it is unknown if incorporation of orthogneiss xenoliths into the massive sulphides occurred largely adjacent to the present position of the massive sulphides, in the parental magma chamber or en route between the two. A post-emplacement deformation event overprinted the MBZ and caused local massive sulphide relocation into the adjacent country rock.

The thickness of MGN, a major host for the disseminated sulphides, progressively decreases from the western end of Babel towards the east (Fig. 7). A change in the conduit orientation from SW to E–W (Fig. 4) could have caused changes in magma velocity, which in turn, would have played a major part in disseminated sulphide precipitation and preservation predominantly at the western end of the conduit. Alternatively, the magmatic head during MGN emplacement may have been waning and, as flow is inferred to be from the southwest, could cause reduction in this unit eastwards. However, a similar decrease in the abundance of disseminated sulphides in the VLGN units towards the east is lacking, and this unit is equally prospective for its entire length. This suggests that sulphide deposition and preservation are associated with magma flow regimes and dynamics, combined with the geometry of the chonolith. Ultimately, the sulphides in the Nebo–Babel system have a primary magmatic origin, but have not accumulated through in situ gravitational settling.

Conclusions

Field, petrological, and geochemical studies presented here lead to the following conclusions:

1. The Nebo–Babel Ni–Cu–PGE deposit, the most significant Ni sulphide discovery to date associated with the Giles Complex and Warakurna LIP in central Australia, is hosted in a low MgO, relatively evolved, essentially olivine-free, tube-like, gabbronorite intrusion that was emplaced into amphibolite facies, sulphide-free granitic gneiss.
2. The tube-like intrusion is interpreted to represent an originally continuous magma chonolith, with three temporarily distinct magma pulses. The initial magma pulse, which exploited a linear weakness in the country rock, was the most primitive, sulphide-saturated, and emplaced under open system conditions. This pulse formed the walls of the chonolith. Successive mineralised and barren magma pulses, of more fractionated magma, were injected into the hotter and thermally insulated core of the chonolith.
3. After the emplacement and crystallisation of MGN unit, BGN and OAGN magma pulse(s) were emplaced and closed system crystal fractionation produced systematic mineralogical and chemical trends mirrored by those observed within these units. We favour a normal fractionation process followed by overturning, and offset, the latter related to the Jameson Fault, thus creating the apparent 'reverse' fractionation described in this contribution.
4. Evidence collected to date indicates that local crustal S addition did not play an important role in achieving sulphide immiscibility, although crustal assimilation may have occurred at a deeper crustal level before magma entering the Nebo–Babel intrusion.
5. Contact relationships indicate that known massive sulphides are late in the sequence of emplacement events. Moreover, the chemistry and Cu tenor of massive sulphides are different to those of the disseminated sulphides, strongly suggesting that the former have undergone sulphide fractionation.
6. The majority of mineralisation drilled to date is in the form of primary magmatic, disseminated sulphides. The main controls on the distribution of disseminated sulphides appear to have been chonolith geometry combined with magma flow regimes and dynamics. In particular, changes in orientation or thickness of the chonolith appear to have been critical in influencing the effectiveness of formation and preservation of disseminated sulphides.

Acknowledgements We wish to thank all geoscientists, both past and present, from WMC Resources and BHP Billiton, who have been involved in the West Musgrave Project since 1995. This work was built on their considerable effort over many years, in particular, Roland Goodgame, Jim McCluskey, and Libby Fontaine. Recent work by Brett Davis has significantly advanced understanding of the structural history at the Nebo–Babel deposit.

We thank Bill Stone for the initial supervision of the project, Steve Barnes for discussions on trapped silicate–liquid crystallisation, Greg Hitchen for assistance with microprobe analyses, and all the people who provided help at the Nebo–Babel field camp. Dave Burrows and Franco Pirajno are thanked for the helpful and constructive reviews.

Z. S. is supported by an Australian Post-graduate Research Award and a Minerals and Energy Research Institute of Western Australia (MERIWA) Scholarship. Financial support for fieldwork and chemical analyses was provided primarily by WMC Resources and, subsequently, BHP Billiton, as well as MERIWA and a Society of Economic Geologists Grants to Z. S., all of which are gratefully acknowledged. We thank BHP Billiton for permission to publish this paper.

References

Baker PM, Waugh RS (2005) The role of surface geochemistry in the discovery of Babel and Nebo magmatic nickel–copper–PGE deposits. Geochem Explor Environ Anal 5:195–200

Ballhaus CG (1993) Petrology of the layered mafic/ultramafic Giles Complex, western Musgrave Block, Western Australia. Australian Geological Survey Organization, p 75, Rec 1992/73

Ballhaus CG, Berry RF (1991) Crystallization pressure and cooling history of the Giles Layered Igneous Complex, Central Australia. J Petrol 32:1–28

Ballhaus CG, Glikson AY (1989) Magma mixing and intraplutonic quenching in the Wingelina Hills Intrusion, Giles Complex, central Australia. J Petrol 30:1443–1469

Ballhaus CG, Glikson AY (1995) The petrology of layered mafic–ultramafic intrusions of the Giles Complex, western Musgrave Block, Western Australia. In: Glikson AY (ed) The Giles mafic–ultramafic complex and environs, western Musgrave Block, central Australia. AGSO J Geol Geophys 16:1–2:69–91, thematic issue

Barnes SJ (1986) The effect of trapped liquid crystallization on cumulus mineral compositions in layered intrusions. Contrib Mineral Petrol 93:524–531

Barnes S-J, Maier WD (1999) The fractionation of Ni, Cu and the noble metals in silicate and sulphide liquids. In: Keays RR (ed) Dynamic processes in magmatic ore deposits and their application in mineral exploration. Geol Assoc Can XIII:69–106, short course notes

Barnes S-J, Naldrett AJ, Gorton MP (1985) The origin of fractionation of platinum-group elements in terrestrial magmas. Chem Geol 53:303–323

Bates RL, Jackson JA (eds) (1987) Glossary of Geology. American Geological Institute, p 788

Brown GM (1957) Pyroxenes from the early and middle stages of fractionation of the Skaergaard intrusion, East Greenland. Mineral Mag 31:511–543

Camacho A (2002) Isotopic test of a thermally driven intraplate orogenic model, Australia. Geology 30:887–891

Camacho A, Fanning CM (1995) Some isotopic constraints on the evolution of the granulite and upper amphibolite terranes in the eastern Musgrave Block, central Australia. Precambrian Res 71:735–751

Camacho A, McDougall I (2000) Intracratonic, strike-slip partitioned transpression and the formation and exhumation of eclogite facies rocks: an example from the Musgrave Block, central Australia. Tectonics 19:978–996

Camacho A, Compston W, McCulloch M, McDougall I (1997) Timing and exhumation of eclogite facies shear zones, Musgrave Block, central Australia. J Metamorph Geol 15: 735–751

Campbell IH (1978) Some problems with the cumulus theory. Lithos 11:311–323

Clarke GI, Buick IS, Glikson AY, Stewart AJ (1995) Structural and pressure temperature evolution of host rocks of the Giles Complex, western Musgrave Block, central Australia. In: Glikson AY (ed) 1995 The Giles mafic–ultramafic complex and environs, western Musgrave Block, central Australia. AGSO J Geol Geophys 16(1–2):25–40, thematic issue

Cox KG, Bell JD, Pankhurst RJ (1979) The interpretation of igneous rocks. G. Allen, London, p 450

Daniels JL (1974) Geology of the Blackstone Region Western Australia. Bull Geol Surv W Aust 123:257

Glikson AY, Ballhaus CG, Clarke GL, Shearton JW, Stewart AJ, Sun S-S (1995) Geological framework and crustal evolution of the Giles mafic–ultramafic complex and environs, western Musgrave Block, central Australia. In: Glikson AY (ed) The Giles mafic–ultramafic complex and environs, western Musgrave Block, central Australia. AGSO J Aust Geol Geophys 16(1–2):41–69, thematic issue

Glikson AY, Stewart AT, Ballhaus GL, Clarke GL, Feeken EHT, Leven JH, Sheraton JW, Sun S-S (1996) Geology of the western Musgrave Block, central Australia, with reference to the mafic–ultramafic Giles Complex. AGSO Bull 239:206

Goode ADT (1977) Intercumulus igneous layering in the Kalka layered intrusions, central Australia. Geol Mag 114:215–218

Goode ADT, Moore AC (1975) High pressure crystallization of the Ewarara, Kalka and Gosse Pile Intrusions, Giles complex, central Australia. Contrib Mineral Petrol 51:77–97

Gray CM (1978) Geochronology of granulite facies gneisses in the western Musgrave Block, central Australia. J Geol Soc Aust 25:403–414

Gray CM, Compston W (1978) A Rb–Sr chronology of the metamorphism and prehistory of central Australian granulites. Geochim Cosmochim Acta 42:1735–1748

Gray CM, Goode ADT (1989) The Kalka layered intrusion, central Australia: a strontium isotopic history of contamination and magma dynamics. Contrib Mineral Petrol 103:35–43

Hunter RH (1987) Textural equilibrium in layered igneous rocks. In: Parsons I (ed) Origins of igneous layering. Reidel, Dordrecht, pp 473–503

Irvine TN (1982) Terminology for layered intrusions. J Petrol 23:127–162

Kretz R (1983) Symbols for rock forming minerals. Am Mineral 68:277–279

LeMaitre (ed) 2002 Igneous rocks, a classification and glossary of terms, 2nd edn. Cambridge Univ. Press, p 236

Li C, Naldrett AJ (1993) Sulphide capacity of magma: a quantitative model and its application to the formation of sulphide ores at Sudbury. Econ Geol 88:1253–1260

Li C, Naldrett AJ (1999) Geology and petrology of the Voisey's Bay intrusion: reaction of olivine with sulphide and silicate liquids. Lithos 47:1–31

Li C, Naldrett AJ (2000) Melting reactions of gneissic inclusions with enclosing magma at Voisey's Bay, Labrador, Canada: Implications with respect to ore genesis. Econ Geol 95(4):801–814

Lightfoot PC, Naldrett AJ (1994) Proceedings of the Sudbury–Noril'sk Symposium. Ont Geol Surv Spec Vol 5:423

Mabuko MAH, Williams IS, Compston W (1996) Zircon U–Pb chronometry of the pressure and temperature history of granulites in the Musgrave Ranges, Central Australia. J Geol 99:675–697

MacDonald GA (1968) Composition and origin of Hawaiian lavas. Mem Geol Soc Amer 116:477–522

Mathison CI (1987) Cyclic units in the Somerset Dam layered gabbro intrusion, southeastern Queensland, Australia. Lithos 20:187–205

McBirney AR, Hunter RH (1995) The cumulate paradigm reconsidered. J Geol 103:114–122

Misra KC, Fleet ME (1973) The chemical composition of synthetic and natural pentlandite assemblages. Econ Geol l68:518–539

Morris PA, Pirajno F (2005) Mesoproterozoic sill complexes in the Bangemall Supergroup, Western Australia: geology, geochemistry, and mineralization potential. Report 99

Myers JS, Shaw RD, Tyler IM (1996) Tectonic evolution of Proterozoic Australia. Tectonics 15:1431–1446

Naldrett AJ (1999) World-class Ni–Cu–PGE deposits: key factors in their genesis. Miner Depos 34:227–240

Nesbitt RW, Goode ADT, Moore AC, Hopwood TP (1970) The Giles Complex, central Australia: a stratified sequence of mafic and ultramafic intrusions. Geol Soc S Africa Spec Pub 1:547–564

Norrish K, Chappell BW (1977) X-ray fluorescence spectrometry. In: Zussman J (ed) Physical methods in determinative mineralogy. Academic, London, pp 201–272

Norrish K, Hutton JT (1969) An accurate X-ray spectrographic method for the analysis of a wide range of geological samples. Geochim Cosmochim Acta 33:431–453

Parsons I (ed) (1987) Origins of igneous layering. NATO ASI series, mathematical and physical sciences v196. Reidel, Dordrecht, p 666

Raedeke LD, McCallum SI (1984) Investigations in the Stillwater Complex: Part II. Petrology and Petrogenesis of the Ultramafic Series. J Petrol 25:395–420

Ripley EM, Alawi JA (1993) Petrogenesis of pelitic xenoliths at the Babbitt Cu–Ni deposit, Duluth Complex, Minnesota, USA. Lithos 21:143–159

Robinson BW, Ware NG, Smith DGW (1998) Modern electron-microprobe trace-element analysis in mineralogy. In: Cabri LJ, Vaughan DJ (eds) Modern approaches to ore and environmental mineralogy. Inter Mineral Assoc Short Course Series 27:153–180

Scrimgeour IR, Close F, Edgoose CJ (1999) Petermann Ranges, N.T. 1:250 000 Geological Series. Northern Territory Geological Survey Explanatory Notes SG 52-7

Scrimgeour IR, Edgoose CJ, Close DF, Wade BP (2005) The Musgrave province—NT's most underexplored terrane. North Territ Geol Surv Rec 2005–001

Seat Z Geology, Petrology, Mineral and Whole-rock Chemistry, Stable and Radiogenic Isotope Systematics and Ni-Cu-PGE Mineralisation of the Nebo-Babel Intrusion, West Musgrave, Western Australia. PhD dissertation, The University of Western Australia (in prep)

Soffel HC (1991) Paläomagnetismus und Archäomagnetismus. Springer, Berlin Heidelberg New York, p 276

Sun S-S, Sheraton JW, Glikson AY, Stewart AJ (1996) A major magmatic event during 1050–1080 Ma in central Australia and an emplacement age for the Giles Complex. AGSO Res Newsl 17:9–10

Wager LR (1963) The mechanism of adcumulus growth in the layered series of the Skaergaard Intrusion. Min Soc Am Spec Pap 1:1–9

Wager LR, Brown GM, Wadsworth WJ (1960) Types of igneous cumulates. J Petrol 1:73–85

White RW, Clarke GL, Nelson DR (1999) SHRIMP U–Pb zircon dating of Grenville-age events in the western part of the Musgrave Block, central Australia. J Metamorph Geol 17:465–481

Wilson AH (1992) The geology of the Great Dyke, Zimbabwe: crystallization, layering, and cumulate formation in the P1 pyroxenite of the Darwendale Subchamber. J Petrol 33:611–664

Wingate MTD, Pirajno F, Morris PA (2004) The Warakurna large igneous province: a new Mesoproterozoic large igneous province in west-central Australia. Geology 32:105–108